

## Micro-computed tomography of the fired clay venus of Dolní Věstonice (Czech Republic)



Petr Neruda <sup>a,\*</sup>, Petr Hamrozi <sup>a</sup>, Zuzana Patáková <sup>b</sup>, Grzegorz Pyka <sup>b</sup>, František Zelenka <sup>b</sup>, Šárka Hladilová <sup>c</sup>, Martin Oliva <sup>a</sup>, Eva Orságová <sup>d</sup>

<sup>a</sup> Moravian Museum, Historical Museum, Anthropos Institute, Brno, 659 37, Czech Republic

<sup>b</sup> Thermo Fisher Scientific, Brno, 627 00, Czech Republic

<sup>c</sup> Masaryk University, Faculty of Science, Department of Geological Sciences, Brno, 611 37, Czech Republic

<sup>d</sup> Brno University of Technology, Faculty of Electrical Engineering and Communication, Department of Biomedical Engineering, Brno, 616 00, Czech Republic

### ARTICLE INFO

#### Keywords:

Palaeolithic art  
Burnt clay  
 $\mu$ -CT scan  
Ceramic composition  
Ceramic matrix provenance  
Shaping technology  
Venus taphonomy  
Gravettian

### ABSTRACT

Small figurines made from fired clay belonging to the Gravettian (Pavlovian) culture (30–25 ka cal BP) represent one of the main forms of spectacular Palaeolithic art. The most well-known example is the Venus from Dolní Věstonice I in the Czech Republic, which is the biggest and best-preserved human figurine made from clay. Due to its high cultural value, exploration of the internal structures of this figurine has represented a huge challenge, as only non-destructive methods could be applied. Thanks to tremendous technological advancements, we were able to use high-resolution micro-CT imaging. This imaging revealed the structural compositions of the ceramic paste, the technology of the statuette's shaping procedure, and the taphonomy of this piece of art. We reveal that the ceramic paste was prepared from loess sediment containing stones, microfossils, and carbonate aggregates from the basement complex as an natural admixture. The particles are randomly distributed. We did not find any bones or ivory remnants inside the body. Missing joined areas of different parts of the body of the Venus indicate that the figurine was made from a single piece of clay using the non-additive method of shaping. The internal cracks in the body of the Venus statuette represent the main feature of its taphonomy and influence the way it will be manipulated in the future.

### 1. Introduction

The discovery of X-rays by Wilhelm Konrad Röntgen in 1895 was a massive scientific advancement. X-rays have been used not only in the field of medicine but also widely applied across archaeological and anthropological research. The first practical use of this method was documented just one year after their discovery (Fiori and Nunzi, 1995; Hughes, 2011). The applicability of X-ray radiography to a range of different materials soon drew the attention of other specialists such as researchers specialising in ceramics, which is arguably the most common material among archaeological findings (for overview see Berg and Ambers, 2016). Thanks to X-rays, a new methodological approach to classifying ceramics by tempers was used for the first time in 1935 (Titterington, 1935). Other research also focused on analyses of tempers and documentation of vessel manufacturing methods (Shepard, 1956; Van Beek, 1969). The groundbreaking work of Rye showed the full potential of radiography (Rye, 1977). This has been followed by many

other studies (Braun, 1982; Carr, 1990, 1993; Carr and Komorowski, 1990).

A subsequent advancement in the field of radiography was the invention of X-ray computed tomography (CT). In addition to a frontal view of an object, as with regular X-rays, CT can also “slice” through an object, providing the researcher with cross-sectional views (Berg and Ambers, 2016). An often used technique is medical computed tomography (e.g. Anderson and Fell, 1995; Applbaum and Applbaum, 2005), which provides a widely accessible non-destructive low-cost technique (Berg and Ambers, 2016). However, the image resolution is not sufficient for certain analyses. X-ray microtomography ( $\mu$ -CT) allows 2D and 3D output even in micrometres, unlike a normal medical scanner with lower sensitivity capabilities (e.g. Landis and Keane, 2010). The effectiveness of  $\mu$ -CT is mainly in specific edge cases where thin sections are not possible (for this issue e.g. Kozatsas et al., 2018). The high sensitivity of  $\mu$ -CT has wide applicability across a variety of ceramic objects in archaeology. This method allows researchers to gain more detailed data

\* Corresponding author.

E-mail address: [pneruda@mzm.cz](mailto:pneruda@mzm.cz) (P. Neruda).

while enabling them to solve more perplexing scientific issues, namely, a study of pores in historical bricks (Reedy and Reedy, 2022a, 2022b), 3D orientation particles and void analysis for identification of hand-built forming techniques (Gait et al., 2022), or other studies focused on the technology and internal structures of ceramics (Bernardini et al., 2019; Kahl and Ramminger, 2012; Kozatsas et al., 2018).

The use of CT technology is crucial for the analysis of many prehistoric artefacts, especially pieces of art. Considering their uniqueness and the high level of protection they are subjected to, any use of destructive techniques such as thin sections is impossible. This is, in particular, true in the case of Palaeolithic artefacts, due to their scarcity and fragility. The application of non-destructive  $\mu$ -CT imagery represents the only effective way of obtaining quantitative and qualitative data regarding the internal structures of highly valued objects (Farbstein and Davies, 2017; Vigorelli et al., 2022). Apart from the non-destructive character of this method, there is another benefit as opposed to the thin section method, which is the capability of exploring the full volume of an object, which is particularly useful for different types of spatial or clustering analysis. This technique was widely applied to post-Palaeolithic figurines and other objects (e.g. Insoll et al., 2016; Kreiter et al., 2014; Pavel et al., 2013; Pizzeghello et al., 2015). Nevertheless,  $\mu$ -CT is still relatively little used for statuettes from the Palaeolithic period. One of the first cases of use of this method was an analysis of the limestone provenience for creating the Willendorf Venus (Weber et al., 2022). Unlike ceramic objects, the internal composition of this rock material could not be adjusted by humans in any way. Regarding ceramic objects, not only the shape but also the composition of ceramic paste and the processing technology could have been subjected to the creator's preferences. Despite the huge research potential of Palaeolithic figurines, micro CT has been only used on pellets from Dolní Věstonice I (cf. info in Farbstein and Davies, 2017). Considering this scarcity of scientific papers using this  $\mu$ -CT technique, this study aims to use this opportunity and shed new light on this issue by exploring the material and internal composition of the Venus of Dolní Věstonice.

### 1.1. Site location and history of research

The complex Gravettian station of Dolní Věstonice I is located in the southeast part of the Czech Republic, approx. 35 km from the city of Brno (Fig. 1:B) on the northeastern slopes of the Pavlov Hills by the river Dyje (Thaya), where the huge Nové Mlýny reservoir was built in the last century. (Fig. 1:C). Dolní Věstonice I is part of an extensive cluster of several Gravettian sites along the Dyje and includes sites like Dolní Věstonice II, Pavlov I, and Pavlov II (Fig. 1:D), among others.

This site is divided into four areas (Fig. 1:D), that lie approx. between the contour lines 180–240 m a.s.l. From the point of view of the researched issue, the most important part is the so-called Upper part, where the Venus of Dolní Věstonice was found. Other fragments of stylistically identical Venuses were also found in the Middle and Up-permost part of the station (Fig. 1:D). The archaeological layer in Dolní Věstonice I is located in the basal part of the loess complex, while in many places it touches the underlying Tertiary sediments, into which weathered Jurassic limestone bedrock is mixed (Klíma, 1963, 1981; Svoboda et al., 2018).

The history of research in Dolní Věstonice I is vast (for this topic see Oliva, 2014; Svoboda, 2020). The first systematic excavations were carried out in 1924 by Karel Absolon (Absolon, 1938a, 1938b; Absolon and Zapletal, 1945), who continued the work of several amateur archaeologists from the years 1922 and 1923. During the years of 1939 and 1942, the archaeological site came under Nazi research funded by the Ahnenerbe Institute, which focused on the origin of the Germans. The research was conducted under the leadership of Assien Bohmers. After the end of the war, the excavation was again taken over by Czech archaeologists, initially by Karel Žebera in 1945 and 1946 (Knor et al., 1953) and afterwards by Bohuslav Klíma, who focused on this site intermittently from 1947 to 1979 (Klíma, 1963, 1981, 1983). In 1990

and 1993, Jiří Svoboda carried out an excavation of several test pits (Svoboda et al., 2018). In the upper part of the site, in the area of the old Klíma test pits from the mid-60s, Martin Novák began new research in 2022, under the patronage of ERC Consolidator Grant "MAMBA", reg. nr. 101045245 (MAMBA, 2024; Novák et al., 2022).

### 1.2. History of statuette research

The unique statuette, known as the Venus of Dolní Věstonice, was found in Dolní Věstonice I (Czech Republic) on July 13, 1925 during the excavation led by Karel Absolon from the Moravian Museum in Brno (Czech Republic). The discovery was made as a part of a larger excavation of a hearth with dimensions of  $13 \times 5$  m, consisting of a red burned loess layer that covered a thick layer full of ash and charcoal fragments (Absolon, 1938b). Initially, a broken-off part of the right leg was found at this layer. This was followed by the discovery of the rest of the body. The distance between both parts was only 10 cm (in detail in Oliva, 2014). Soft ashes formed a crust on the surface of the artefact. Some parts of the body were also covered in a thin layer of carbonates (Fig. 2:A).

Absolon unimaginably delayed the publication of one of his most outstanding discoveries. The Venus, without an attached picture, was mentioned a year after its discovery and the first good-quality photographs were made public in the world-renowned social journal "The Illustrated London News" on November 30, 1929 (Absolon, 1929). A comprehensive scientific examination and photographic documentation of the Venus was conducted in the second scientific report in 1938 (Absolon, 1938b). However, Absolon did not describe the figurine as ceramic. Based on the chemical analysis of a sample obtained from the mass of the Venus, he determined the material to be a mixture of crushed burnt bones and mammoth tusks mixed with loess that only resembled burnt clay.

The question regarding the material composition and the internal structure of the figurine was difficult to answer due to its uniqueness and high level of safekeeping, which did not allow the use of any kind of destructive methods. The first analysis of the Venus's material composition, in particular a fragment that was broken off the figurine's side, was performed in the late 1980s using X-ray diffraction and an electron beam microprobe. These analyses revealed that the body was created from a local source of Dolní Věstonice coarse-particle loess with only a small amount of clay in it (Vandiver et al., 1989).

However, this approach only brought some information about the material, while the internal structures remained shrouded in mystery until the year 2004, when a medical CT scanner showed some cracks and white spots inside the Venus body. The white spots represent a material with a higher density compared to the rest of the body. Nevertheless, other detailed analyses were not performed, and the scan results did not provide many new insights (Hložek et al., 2008).

## 2. Methods

### 2.1. Research objectives

Our goal was to address several questions related to the analysis of the Venus and other ceramic figurines by using  $\mu$ -CT scanning.

- 1) What is the composition of the ceramic paste?
  - a. Was Absolon's idea about the appearance of mammoth bone fragments inside the ceramic paste correct?
  - b. Is there any admixture in the ceramic paste that can be considered direct evidence of placing inclusions into the paste for symbolic reasons?
  - c. What is the distribution of inclusions and what are their attributes?
- 2) Are we able to specify the sediment provenience used for making the ceramic paste?

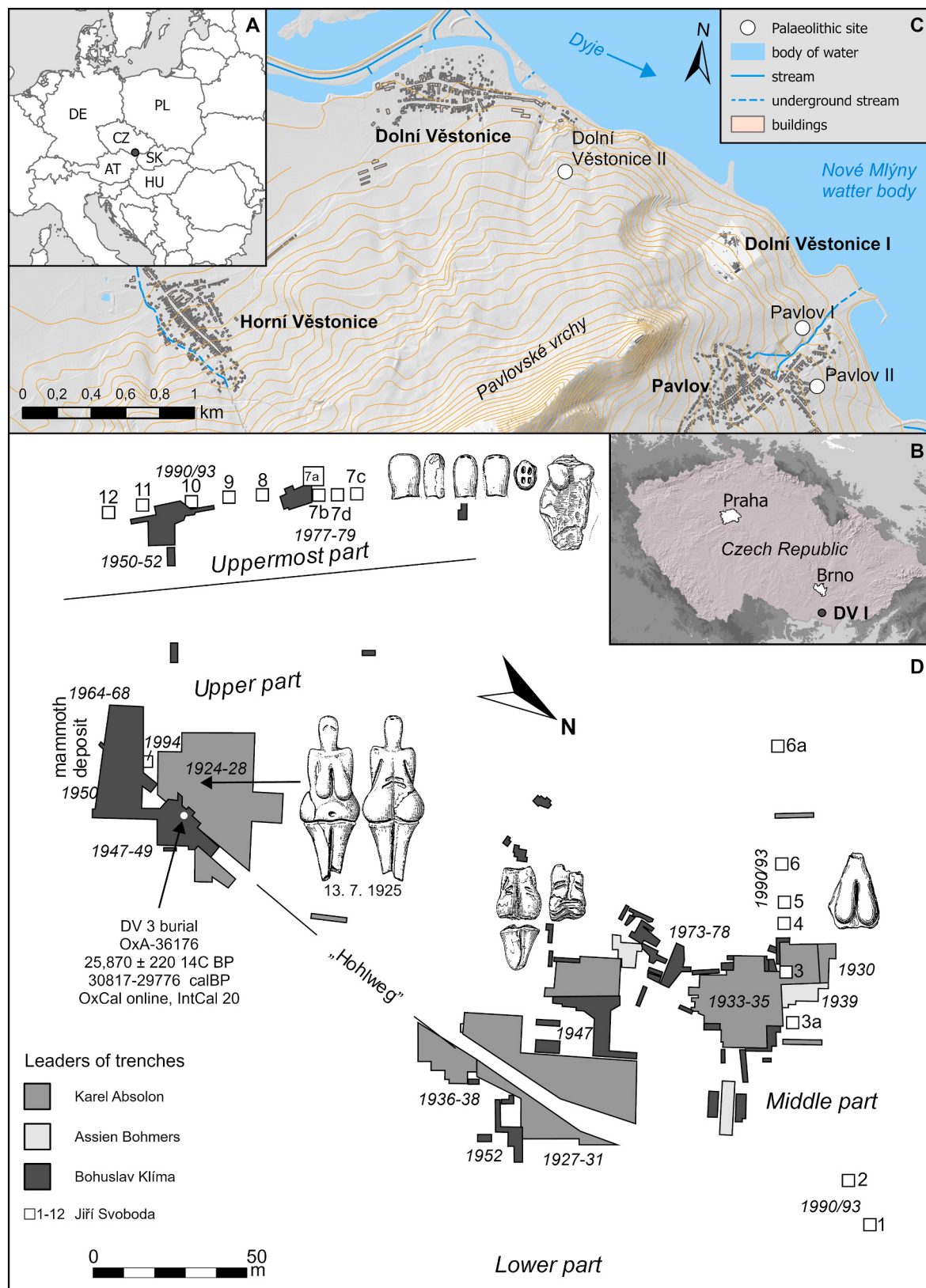


**Fig. 1.** Location of Dolní Věstonice I on an inset map of Europe (A), the Czech Republic (B), and regions of Dolní Věstonice – Pavlov (C). Plan of Dolní Věstonice I with marked areas where researchers unveiled the Venus and other fragments of analogous shape (D; modified according to (Svoboda, 2020; Oliva, 2014). Map P. Neruda, with the use of DMR5G (ČÚZK, 2017), water sources and buildings (ČÚZK, 2021), and SRTM90mDEMver4 (Jarvis et al., 2008).

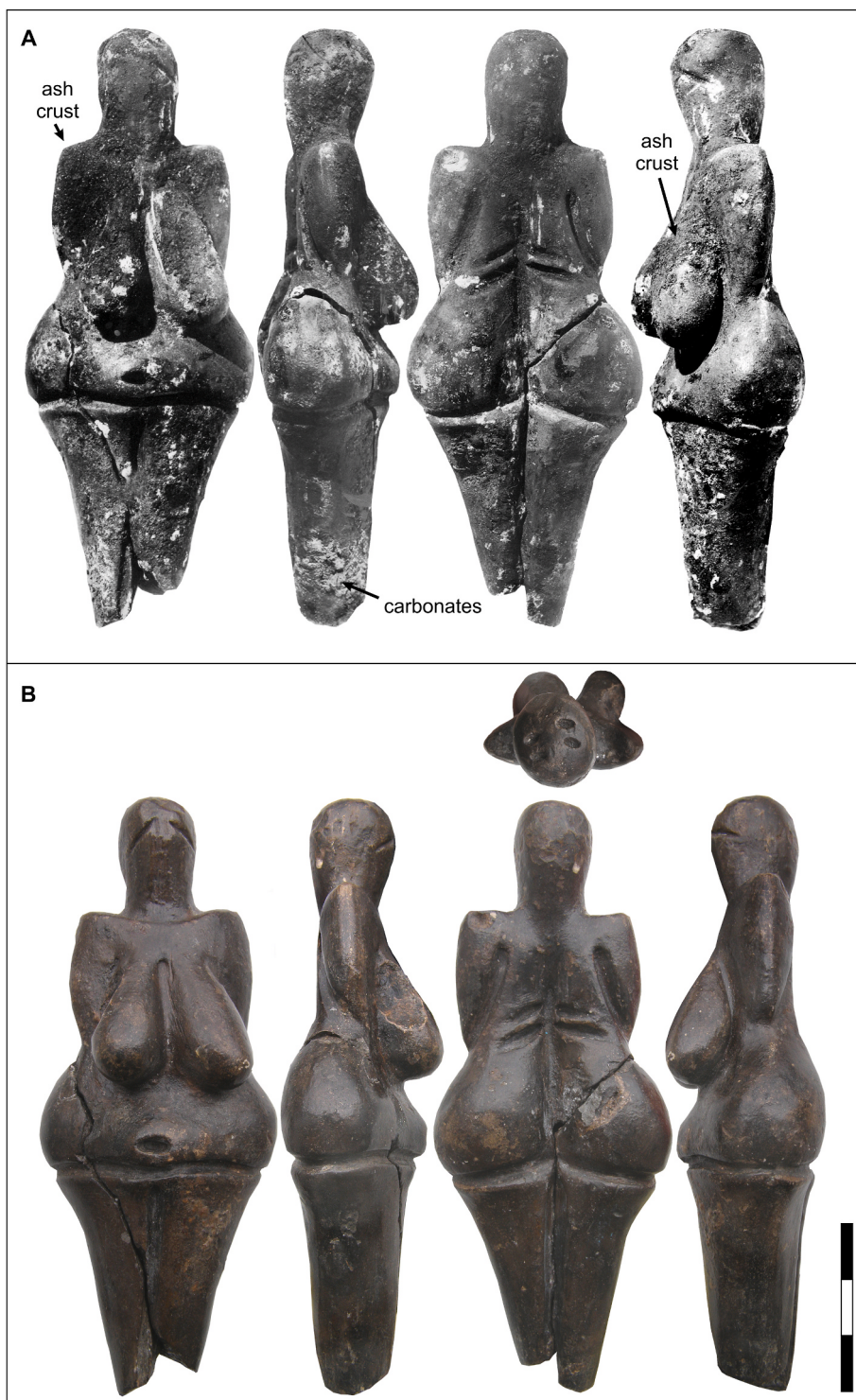


**Fig. 2.** The Venus from Dolní Věstonice. A: the state of preservation at the time of the findings (archive of the Moravian Museum), B: current preservation status (photo O. Kroupa, Moravian Museum).

- 3) Was the figurine manufactured using additive or non-additive technology?
- 4) What is the taphonomy of the Venus?

## 2.2. Statuette settings

The preserved statuette, stored in the Anthropos Institute of the Moravian Museum in Brno, Czech Republic under the ID DV 30000,

consisted of two separated pieces with the refitted body being 111 mm long, and 44 mm wide (Fig. 2:B). The lower part of the legs is missing. The figure is characterised by an oval head with four holes at the top and two grooves representing eyes, large breasts (the right one is slightly damaged), wide hips and fat folds shaped on the back. The hands are only schematically indicated, and the legs were modelled as a single unit but visually distinguished by two vertical grooves on the front and back.

The statuette is not directly dated. To determine its age, only

contextual data collected in the closest vicinity can be used. The only accurately located date from the area of the upper part of the Dolní Věstonice I station was gained by analysing the postcranial remains of a woman from DV3 (Fig. 1:D). The skeleton is dated back to  $25,870 \pm 220$   $^{14}\text{C}$  BP (OxA-36176), allowing us to estimate the age of the figurine in the range of 30,817–29,776 calBP (Nerudová et al., 2019). The results correlate with other data that have been collected from the uppermost and middle part of the site (Svoboda, 2020).

### 2.3. $\mu$ -CT scanning of venus

To analyse the internal structure of the statue, we chose CT technology using X-rays. This is non-destructive imaging, where different materials absorb X-rays differently, thus making it possible to visually distinguish them from each other. The method itself does not result in a chemical analysis of the material. Therefore, we also scanned artificially created phantoms that contained material fragments, the presence of which we expected to find in the Venus itself. We were inspired by medical diagnostic methods, where this procedure is used to refine the material analysis of a sample (McGarry et al., 2020; Shikhaliyev, 2012).

For the scan of the statue itself, we chose a helical (spiral) trajectory and acquisition scheme, which is suitable for iterative data reconstruction. The scanning was performed on 17. 8. 2016 in Brno (Czech Republic) on a HeliScan microCT scanner developed by Thermo Fisher. At the time of scanning, the scanning area of the scanner did not allow the entire Venus to be scanned. The scan was divided into two parts, which required a specific technical solution.

#### 2.3.1. Scanning pretreatment – a sample holder

An essential requirement for successful tomography data acquisition is to minimise the uncontrolled sample movement during scanning. HeliScan uses geometrical magnification to form the image. Therefore, the sample holder must allow for close proximity between the sample and the X-ray source to enable optimal scanning resolution. Material with low X-ray attenuations was preferred in order to optimise the X-ray flux and spectra impacting the sample. These limitations led us to develop the unique sample holder for the Venus, which was made from polyethylene foam shaped to the outer diameter of the cylinder. We split the holder into two halves and based it on a plaster model of the Venus, the negative copy of its shape was carved into the foam to provide secure housing for the statuette. To enable scanning of the Venus and material phantoms under the same conditions, two additional compartments for phantoms were created in the same holder (Fig. 3:A). The foam holder was then secured by gauze and the bottom third was inserted into a

plastic cap mounted on a standard HeliScan sample holder (Fig. 3:B).

#### 2.3.2. Data acquisition

Before scanning the archaeological artefact, which is subjected to a high level of safekeeping, test scanning was conducted on a plaster cast of the Venus. It was necessary to verify whether the sample mounting was sufficiently robust and at the same time optimise the parameters of the acceleration voltage along with exposure time.

To secure good resolution and contrast, several test scans were performed using similar materials and geometry, but without scanning the actual Venus itself, so that potential physical strain on the statuette was minimised. This allowed us to verify that the sample mounting was sufficiently robust and also to optimise the parameters of the acceleration voltage and exposure time.

We opted for a scan strategy using the space-filling trajectory (Kingston et al., 2018), where X-ray projections were acquired from directions uniformly distributed onto an imaginary cylindrical surface surrounding the artefact. This trajectory allowed us to scan elongated samples with a relatively large aspect ratio in a continuous scan without potential stitching artefacts. Due to the scale of the statuette, a multiscan approach was applied. The upper and lower parts of the Venus were scanned separately with an overlapping region captured in both scans for accurate merging purposes. This allowed us to maximise the resolution and overcome the vertical translation stage travel range limitation of 100 mm. This left one overlapping region in the final image of the complete sample.

#### Key acquisition parameters.

- Acceleration voltage: 110 kV
- Beam current: 60  $\mu\text{A}$
- Exposure time: 2.3 s per projection (accumulative)
- Number of projections per revolution: 1800
- Beam filtering: 0.1 mm of stainless steel
- The geometry of the scan was chosen to target voxel size 19  $\mu\text{m}$  or lower.

A total of 7500 X-ray projections were collected from the statue and divided into two disjoint space-filling trajectories. From this, a digital 3D representation of the statuette was formed using an iterative reconstruction algorithm specifically designed to take advantage of the projection angle distribution of the space-filling trajectory to generate a geometrically faithful representation of tall samples (Varslot et al., 2011). To compare the known composition and structure of the phantoms with that of the Venus figurine, it was crucial to minimise effects to

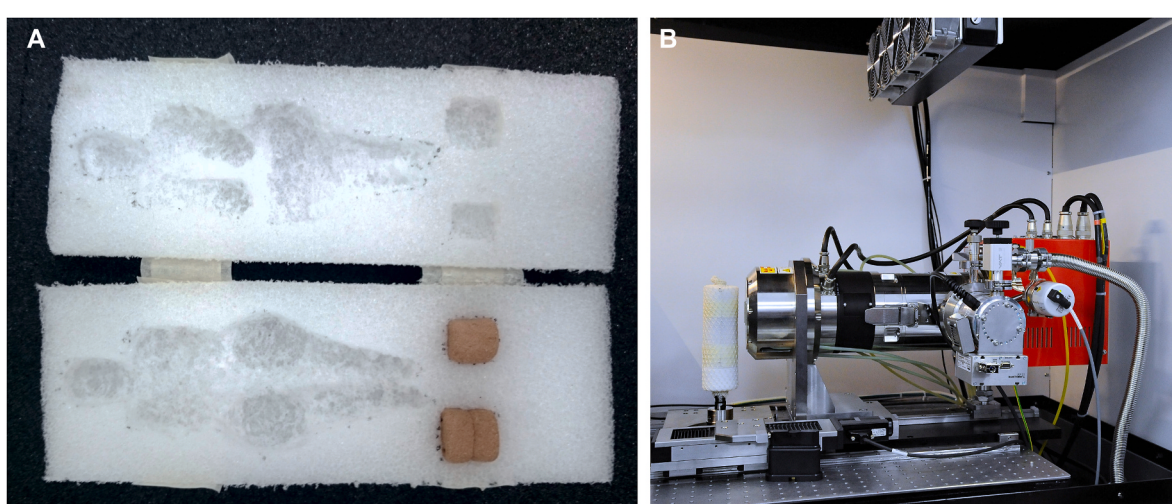


**Fig. 3.** A – Polymeric foam (polythene) case used for scanning the Venus and 2 material phantoms (ID, 2016/1 and 2016/2); B - Placement of the Venus figurine in the holder inside the HeliScan scanning chamber. The steel pivot at the bottom of the holder enables shifting of the holder up and down (photos Z. Patáková).

avoid streak artefacts around dense inclusions in the statue. Therefore, the 0.1 mm stainless steel filter was used to filter out the lower-energy X-rays from the spectrum applied on the statue. The material and thickness of the filter were determined during the testing scans as we were optimizing the intensity of the signal on the detector vs. exposure time and X-ray filtering. The output is a voxelised greyscale representation of the statue. The final length of an edge of a voxel was 18.54 µm.

#### 2.4. Reference samples

To address the defined research goals, it was crucial to compare the obtained results from the figurine with the reference samples, which contained inclusions that were expected to be found inside the Venus based on our previous insights. Some of the used phantoms carried specific properties to account for different modification methods applied to the figurine. These modifications encompass punctures into wet material or a conjoint area between two pieces of material. In total, 3 sets of phantoms were made to document the process of this research (Tab. 1; Appendix B; Fig. 8). In all cases, the loess sediment from Dolní Věstonice II (WGS-84: 48.8839939 N, 16.6548236 E) was used to closely replicate the original wet ceramic paste, even containing various inclusions and subjected to different forming techniques.

The first set (Table 1:2016/1 and 2016/2) was scanned directly with the Venus and consisted of two cylinders made from Dolní Věstonice loess. One cylinder contained carbonates separated from the loess by floating. The same loess was used for the second phantom and contained weathered fossil bones and fossil mammoth ivory. Both phantoms were burnt on a laboratory stove at a temperature of 600 °C. Both bone and ivory changed structure into a form of charcoal.

The second phantom set was scanned in 2019 after the first preliminary analysis of the Venus composition. Because the fossilised bone and mammoth tusk turned into coal remnants, we were not able to investigate their internal structures using micro CT. For this reason, a pair of new phantoms, containing fresh bone fragments and recent elephant ivory (Table 1:2019/1 and 2016/2), was created. The ivory was a remnant from an experiment by Sebastian Pfeifer from Friedrich Schiller University in Jena, who registered it as ID 1001 (Pfeifer et al., 2019). The first phantom (2019/1) was heated to 400 °C and the second one (2019/2) to 600 °C to compare differences in the preservation of both organic materials. Both phantoms were made of two separate parts. The wetted parts were merged either using pressure or a twisting movement. Fragments of charcoal were expected in the ceramic paste; therefore, a huge piece of charcoal originally found in the waste material during MZM research on the Mesolithic site in Smolín (Table 1:2019/3) was placed inside a loess phantom. In this context, the sample's surface was subjected to punctures made into the dry ceramic material by the quill part of a feather.

Phantom 2019/4 contained several small charcoals that we separated from the original archaeological layer from Dolní Věstonice that is preserved in the collection of the Moravian Museum in Brno. The exact location in the context of the site is unknown, but most likely we are dealing with one of the samples collected during the B. Klíma excavation carried out in the 1940s (Table 1:2019/4). The hard inorganic material was taken from the same sediment for the purpose of checking its appearance on CT images and comparing them to the fragments of rocks found inside the Venus. In addition to this organic material, experimental chipped fragments made from flint and small pieces of quartz (Table 1:2019/5 and 2019/6) were also added to this sample set. In the case of quartz and silicates, we wanted to verify how they are represented on the CT image, especially with regard to density. Finally, a lump of this sediment was scanned in order to ascertain the porosity of the original archaeological layer (Table 1:2019/7).

In 2020, we extended reference sample scanning to a third set of phantoms (Table 1). Sample 2020/1 contained quartz fragments from a river pebble and a hematite rock from the original archaeological layer from the Dolní Věstonice site. Sample 2020/2 recorded punctures by a

**Table 1**

List of reference samples (phantoms).

Phantom ID	Upper part	Lower part	Temperature of heating (°C)	Applied technological processes related to Venus shaping
2016/1	carbonate concretions			
2016/2	fossil bone	fossil mammoth ivory	600	
2019/1	mammoth ivory ID 1001 <sup>a</sup>	recent bone	400	Two isolated cylinders of a wet ceramic paste simply joined without twisting; smoothing of the surface
2019/2	mammoth ivory ID 1001 <sup>a</sup>	recent bone	600	Two isolated cylinders of a wet ceramic paste joined by twisting; smoothing of the phantom surface
2019/3	Charcoal (Mesolithic Age) <sup>b</sup>		600	A row of punctures into a semi-dry ceramic paste
2019/4	Charcoal from an original archaeological layer		600	
2019/5	Small stones from a cultural layer	Three small silicate flakes (artificially knapped)	600	Four punctures by a feather shaft into the surface of wet ceramic paste smoothed by ivory (imitation of the surface finishing); two grooves, resembling the eyes of Venus on the surface and three small flint flakes
2019/6	A lump of hematite	Four grains of quartz	600	
2019/7	A lump of the original archaeological layer		not burnt	testing of the original content
2020/1	Hematite from the archaeological layer	Quartz fragments from river pebble	600	
2020/2			600	Four punctures by a bird feather on the top of the head and two engraved grooves imitate eyes; the semi-dry ceramic paste

<sup>a</sup> Provided by S. Pfeifer.

<sup>b</sup> Collection of Anthropos Institute, waste from the excavation in Smolín. For images see Appendix B Fig. 8.

bird feather into the semi-dry ceramic matrix shaped to the form of a head. Two grooves appeared to be imitating the eyes of the Venus.

#### 2.5. Image processing and segmentation of particles

There were two stages in the segmentation of the particles inside the

Venus. For the morpho-statistical analysis, we used the complete model of Venus conjoined from the two scanned parts of Venus. The inner particles in the 3D scan of the Venus body were segmented based on their brightness, which is given by the material absorption of the X-ray beam. All selected particles were recorded as independent material and later manually edited using tools for segmentation available in Avizo software. This was especially necessary for the parts near the surface, where automatic segmentation was not accurate since the thinner parts of Venus had the optimal histogram shifted to a different range in comparison to the thicker parts, such as the pelvic region. Calcite crystals developed in the cracks as a by-product of the manufacturing

process were manually edited out since they were not part of the original ceramic paste. All inclusions in such an edited model were stored for specific analysis as an individual dataset. Subsequently, a collection of smaller, bright inclusions was singled out from this dataset for the purpose of morphological analysis. In addition, some of these inclusions were also converted into 3D models.

Segmentation of the cracks was conducted through a similar approach. Two 3D models of cracks were rendered, implementing automatic segmentation by utilizing the histogram and subsequently using the manual editing option. The first one included only cavities inside the body, and the second one included cracks that were connected

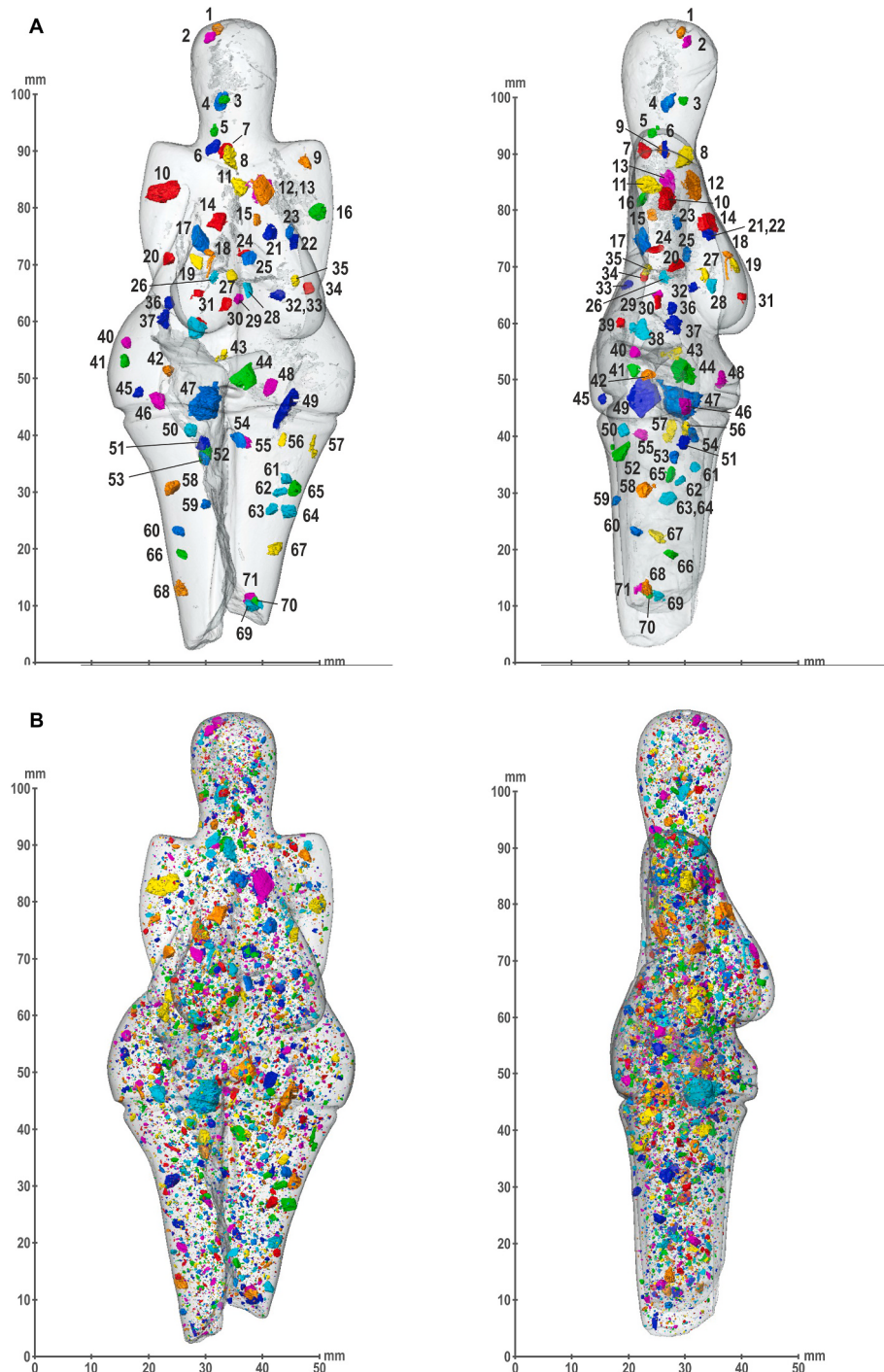


**Fig. 4.** Distribution of particles larger or equal to  $2 \text{ mm}^3$  (A) and  $1 \text{ mm}^3$  (B) in the body of the Venus. Anterior views on the left, right lateral views on the left. Numbers correlate to the numbering of particles (P) in [Appendix B; Figs. 1–7](#). Segmentation and Visualisation by P. Neruda.

to the surface.

To investigate the possible occurrence of mammoth bone remnants and other admixtures, a group of larger inclusions were set apart. Taking into account knowledge already possessed about Gravettian culture, mammoth ivory remnants, animal teeth, or tiny fossils could have been placed inside the figurine for symbolic purposes. Therefore, it was necessary to create a volume constraint for the group of larger inclusions, defined as being the size of an average rice grain, about  $2\text{ mm}^3$ .

Two groups were set apart from the inclusions dataset. The first was a group of inclusions with a volume equal to or larger than  $2\text{ mm}^3$  (Fig. 4: A), and the second one included all inclusions larger than  $1\text{ mm}^3$  in case of possible comparison (Fig. 4:B). All these inclusions were numbered based on their vertical position in relation to the body, ranging from the head to the legs. These numbers were used as an identification for the documentation of these objects, utilizing orthoslices and 3D models in some cases. The documentation of individual inclusions was conducted separately using the upper and lower models of the Venus in the original resolution. The process of segmentation was based on the use of histogram settings according to local conditions, and manual segmentation tools served to increase the selection accuracy of parts affected by histogram shifting.

In the same way, microfossils were segmented, even though their volume was mostly smaller than the defined volume constraint. In this scenario, it was essential to obtain a very accurate 3D model, allowing their taxonomical classification.

## 2. 4. Statistical analyses

The descriptive statistical analysis was applied to the inclusions segmented by semiautomatic segmentation of the model of the Venus. The original dataset for the statistical analysis was generated by Avizo software in Standard Shape Analysis format, which consisted of 102,515 records and 37 different features (see [original dataset](#)). The analysis was performed in several steps (see [Appendix A](#)). Firstly, the dataset was pre-processed, encompassing dropping redundant and erroneous values. Secondly, exploratory data analysis was carried out, gaining insight into data distributions, and basic descriptive statistics were used to provide information about the number of particles, their size, shape, and position in three-dimensional space. In order to obtain an insight into the shape distribution of the segmented inclusions, a spherical index was calculated along with outlining the multidimensional data points dispersed in 3D space by using their coordinates. The aim was to determine whether there was a prevalence of a certain kind of inclusion shape or any obvious clusters. Any obvious cluster or inclusions of a high level of sphericity could indicate intentional manipulation with the ceramic material for specific technological or symbolic reasons.

## 2. 5. Microfossils determination

Given the fact that the segmentation revealed the presence of microfossils in the ceramic material of the Venus, a part of this research focused on their age and location determination in order to interpret their geographical origin. This admixture in the building material of the Venus can indicate the building sediment provenience.

Paleontological objects were studied using orthoimages along with 3D images and were classified based on morphological traits. To determine a stratigraphic classification, the following publications were used: ([Flügel, 2004](#); [Holzknecht and Hamršmid, 1988](#); [Hunter and Underwood, 2009](#); [Jüttner, 1922](#); [Krajewski et al., 2020](#); [Kroh and Lukešeder, 2009](#); [Moore, 1966](#); [Moore and Jeffords, 1968](#); [Müller, 1963, 1980](#); [Murray, 1990](#); [Řehánek, 1987](#); [Řehoř et al., 1978](#); [Salamon et al., 2021](#); [Schneider et al., 2013](#); [Žít and Michalík, 1984](#)).

## 3. Results

### 3.1. Description of large inclusions

The main goal was to determine the composition of the building material with the intention of answering the questions raised about the presence of mammoth ivory and bones or identifying larger inclusions inside the sedimentary material that could have been placed inside for symbolic purposes.

The comprehensive data obtained from scanning the Venus significantly expands our interpretive possibilities. Semi-automatic micro-CT segmentation generated a data file containing 102,515 records. Each record corresponds to a scanned particle with a volume ranging from  $6.78647 \times 10^{-6}\text{ mm}^3$ – $91.7529\text{ mm}^3$ . The initial exploratory analysis of the cleaned dataset, which contained 92,320 records, showed that a large portion of the particles scanned were incredibly small ([Table 2](#)). The average volume was only  $0.011\text{ mm}^3$  (S.D.  $0.381\text{ mm}^3$ , max =  $91.753\text{ mm}^3$ , min =  $0.00001\text{ mm}^3$ ). Although only 133 particles exceed a threshold of  $1\text{ mm}^3$  (Fig. 4:B), they comprise a significant 59.12% of the total volume of all particles. In the case of inclusions  $\geq 2\text{ mm}^3$  (Fig. 4: A), 69 identified items represent 51.9% of the volume of all particles ([Table 2](#)).

Firstly, we investigated whether the  $\geq 2\text{ mm}^3$  particles exhibited any clusters in terms of their position in three-dimensional space, as well as their physical properties such as anisotropy, elongation, flatness, and sphericity (see [Appendix A](#) and [GitHub](#)). Based on the methods used, we did not identify any cluster of inclusions. Subsequently, the issue of particle shapes using the sphericity index values was addressed (see [Appendix A](#) and [GitHub](#)). In the observed group of particles with a particle volume  $\geq 2\text{ mm}^3$ , the average index of sphericity is equal to 0.400 (S.D. 0.082, max = 0.557, min = 0.222), indicating a predominance of uneven and angular shapes.

Based on the results of clustering and the index of sphericity analyses, our main attention was redirected towards the classification of internal structure with a volume  $\geq 2\text{ mm}^3$ . Apart from the 69 particles (Fig. 4:A) that met the volume threshold, a few additional microfossils discovered inside the body of the Venus were analysed along with the particle group. Although the particles exhibit minor variations, they can still be categorised into distinct groups ([Appendix B](#)) by taking into account their shape and internal composition.

The majority of the particles exhibit polyhedral shapes with slightly rounded edges, and they contain prominent veins that are visible on the orthoslices (Fig. 5:P17). These veins are easily distinguishable due to their bright white colour (Group 1; red arrows in [Appendix B](#); Fig. 1). The second group contains inclusions that share the same shape as those in the largest group, but their internal structure tends to be less compact (Group 2; Fig. 5:P13 and red arrows in [Appendix B](#); Fig. 2). The third group of particles is characterised by a strongly disintegrated, porphyritic-like texture. While their shape is similar to that of the two previous groups, their edges are slightly rounded, and the surfaces appear to be eroded (Group 3; Fig. 5:P5 and [Appendix B](#); Fig. 3). The next group of particles is distinguished by a fairly rounded shape and a porphyritic-like texture, which differs from the particles of Groups 1 and 2 (Group 4; Fig. 5:P10 and [Appendix B](#); Fig. 4). The fifth group is

**Table 2**  
Particle quantity and volume overview.

Components	Measurements	
	Count	Volume [ $\text{mm}^3$ ]
Venus body	39,560	
All segmented particles	102515	995.76
All particles without measurement errors	92320	955.66
All particles $\geq 2\text{ mm}^3$	69	496.42
All particles $\geq 2\text{ mm}^3$ without measurement errors	69	496.42
Cracks and porosity	5486	210.18

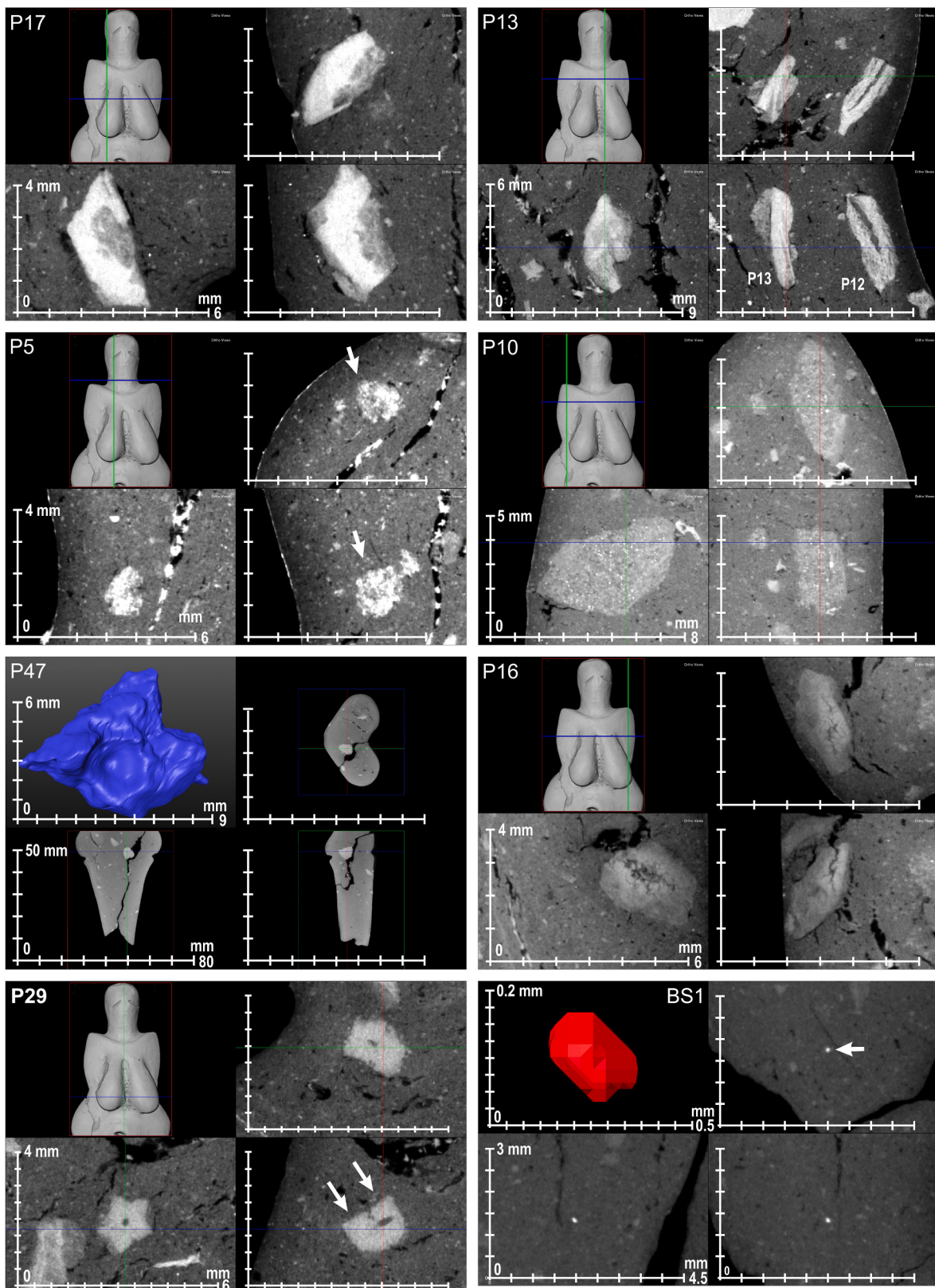


**Fig. 5.** Inclusions overview in the ceramic paste. P17 – group 1, P13 – group 2, P5 – group 3, P10 – group 4, P47 – group 5, P16 – group 6, P29 – group 7, microfossils and BS1 – bright spots, heavy minerals. For more images see [Appendix B](#).

comprised of inclusions with a higher density and irregular shape, sometimes displaying an oval shape and compact texture. (Group 5; Fig. 5:P47 and Appendix B; Fig. 5). The reference calcium carbonate images (Appendix B; Fig. 8:E1) suggest that objects P41 and P47 are likely calcareous nodules, which are commonly found in loess sequences. The sixth group is composed of just two objects; these differ from the previous groups in terms of their oval shape (Group 6; Fig. 5: P16 and Appendix B; Fig. 6). The two objects (Fig. 5:P16; Appendix B; Fig. 6f: P2 and P16) manifest distinct differences in texture. (P2) has two different surface textures, with one part being notably lighter than the other. In contrast, (P16) seems to be relatively uniform in texture but has a minor crack running through it.

Group 7 is distinct from the others by containing fossils with a volume less than  $2 \text{ mm}^3$  (Fig. 5:P29 and Appendix B; Fig. 7). All the identified fossils are generally quite small, with only two of them (Appendix B; Fig. 7:P29 and P39) having a volume larger than  $2 \text{ mm}^3$ . Most of the identifiable fossils in the images belong to the phylum Echinodermata, particularly pluricolumnalia of crinoids (class Crinoidea). The fossils with five-part radial symmetry in the orthophotos P29 and P39 are likely from the order Isocrinida and are typically found in Jurassic deposits. Aside from the Echinodermata fossils, there is also a fragment of a snail from the phylum Mollusca, class Gastropoda, as seen in Appendix B Fig. 7:Px1. Most of the fossils mentioned above were found in Jurassic deposits in the area of Dolní Věstonice, which is part of the Carpathian flysch belt, a tectonic zone stretching from the Danube to the Dyje river in Lower Austria and South Moravia (Jüttner, 1922; Řehánek, 1987; Schneider et al., 2013; Žitt and Michalík, 1984; Appendix B; Fig. 7).

There was a significant emphasis placed on identifying hard animal tissues (HAT), such as bones and mammoth tusks. Their identification should be relatively easy due to their characteristic structures (compare Appendix B; Fig. 8:A and B). HAT reference samples show that the internal structure of bone exhibits small lens-shaped cavities (white arrows in Appendix B; Fig. 8:A1–A5); the remains of a porous structure that represents spongiosa are characteristic (cf. pink arrows in Appendix B Fig. 8:A1-6). Ivory, on the other hand, has a very fine homogeneous structure with indications of lamination (Appendix B; Fig. 8:B1–B5). Fragments of elephant ivory are distinctly angular with sharp edges (Appendix B; Fig. 8:B5). Given these characteristic features, there is no clear evidence of the presence of these HAT inside the Venus. Likewise, no evidence was found of any artefacts that could have potentially appeared in the ceramic paste. However, CT images of the cultural layer from Dolní Věstonice I show, for example, small flakes (Appendix B; Fig. 8:F1–F2). Moreover, the experimentally made pieces demonstrate that their identification is simple because we can see the rest of the striking platform and a bulb (Appendix B; Fig. 8:F3).

### 3.2. Small particle description

Our attention was also drawn to the small inclusions with less than  $2 \text{ mm}^3$ , since the analysis of their spatial distribution or their shapes could indicate the quality of the ceramic paste. Firstly, we attempted to address these questions through clustering analysis, which was applied to the entire cleaned dataset. However, this approach proved to be ineffective due to the majority of particles being extremely small, leading to significant overlap among individual clusters. This means that the distribution of the small inclusions is completely random throughout the whole volume of the body.

Subsequently, the issue of particle shapes was addressed by using the sphericity index values. In the observed group of particles with a particle volume  $\geq 2 \text{ mm}^3$ , the average index of sphericity is equal to 0.400 (S.D. 0.082, max = 0.557, min = 0.222), indicating a predominance of uneven and angular shapes. A sphericity index greater or equal to 0.7 was only found within the particles smaller than  $0.003 \text{ mm}^3$ , which would also include the bright particles randomly distributed across the body of the Venus. For these “bright” particles, the sphericity index mean value is 0.682 (S.D. = 0.0725, max = 0.806, min = 0.381). Upon closer

examination of its form, it bears a resemblance to the shape of a crystal (cf. Fig. 5:BS1 and Appendix B; Fig. 9).

### 3.3. Technological features of the statuette

The obtained  $\mu$ -CT data allows us to study the technological aspects related to the manufacturing process. One of the most addressed issues is the question about the manufacturing technique used, specifically, the usage of additive and non-additive techniques. For this reason, we were looking for any traces showing the joining areas between the extremities and the body. At first, the reference samples made from the loess sediment were used as an attempt to join two pieces at various moisture levels by applying either pressure or a twisting movement. Nevertheless, all the samples showed distinct joining surface areas (red arrows in Fig. 6:F–G). Subsequently, the analysis focused on the figurine itself, namely, the longitudinal slices at the junction of the head and body (Fig. 6:A–D) and transverse slices across the chest area, where breasts could have been attached to the corpus. In both cases, the use of the additive technique represents a certain technological advantage and would have simplified the shaping of the figurine. Even though the connection of two body parts should be easily detectable (Kreiter, 2008), in particular by utilizing high-resolution images, interlayer regions were found that would demonstrate an additive method of creating the figurine (cf. Fig. 6:A–E). Only at the lower edge of the left breast is a crack visible (white arrows in Fig. 6:D and E), which may have formed in areas where a part of the breast was subsequently pressed against the body of the figurine.

The slice images indicated kneading of the ceramic clay, since the pores in the body material are significantly smaller (Fig. 7:A and B) than the pores in the piece of sediment obtained from the original cultural layer (Fig. 7:C). It is evident that on some longitudinal and transverse sections, a hint of layering is visible. This follows the external body shape, which corresponds with the preparation of the ceramic clay (Fig. 7:A and B).

More specifically, we can also address a specific feature preserved on the top of the head of the Venus figurine. There are four holes (Fig. 8:A) whose morphology has not been precisely known until now. The dimensions of the holes range from  $2.7\text{--}2.9 \times 1.1\text{--}1.2 \text{ mm}$ , and the depth is about  $1.5\text{--}1.9 \text{ mm}$  (Fig. 8:D). The white layer at the bottom of the punctures, which is prominently visible in the images as a light colour, represents a secondarily created  $\text{CaCO}_3$  coating (Fig. 8:C). The created 3D model clearly shows that all four holes are similar in shape (Fig. 8:B) and were therefore made with the same pointed tool of a lens-shaped cross-section. Based on the comparison with reference phantoms, we can state that the punctures on the top of the head were made in partially dried ceramic paste because their edges are rounded (cf. white arrows in Fig. 8:F). In the case of wet ceramic paste, a burr is formed along the periphery of the holes (cf. blue and white arrows in Fig. 8:G). In addition to the rounded edges observed around the punctures on the top of the head, rounded edges were also noticed around the eyes (Fig. 8:E) and navel of the Venus figurine.

### 3.4. Taphonomy

An important part of this research is the analysis of the taphonomy of the inner part of the Venus. We had only very limited information about the taphonomy based on images with low resolution. The analysis of the images stressed the concerning number of cracks. The cracks and larger pores in the clay material have a total volume of  $210.18 \text{ mm}^3$  (Table 2), which accounts for 0.5% of the total volume of the figurine. The densest collection of cracks was revealed in the abdominal area (Fig. 9:A3) and chest (Fig. 9:A2, B and D.) Most of the larger cracks are oriented along the longitudinal axis of the entire body (Fig. 9:C). It is clear that there is an extensive crack situated on the left side of the Venus (Fig. 9:C light blue) as well as three smaller ones in the chest area (Fig. 9:C red, orange and yellow).

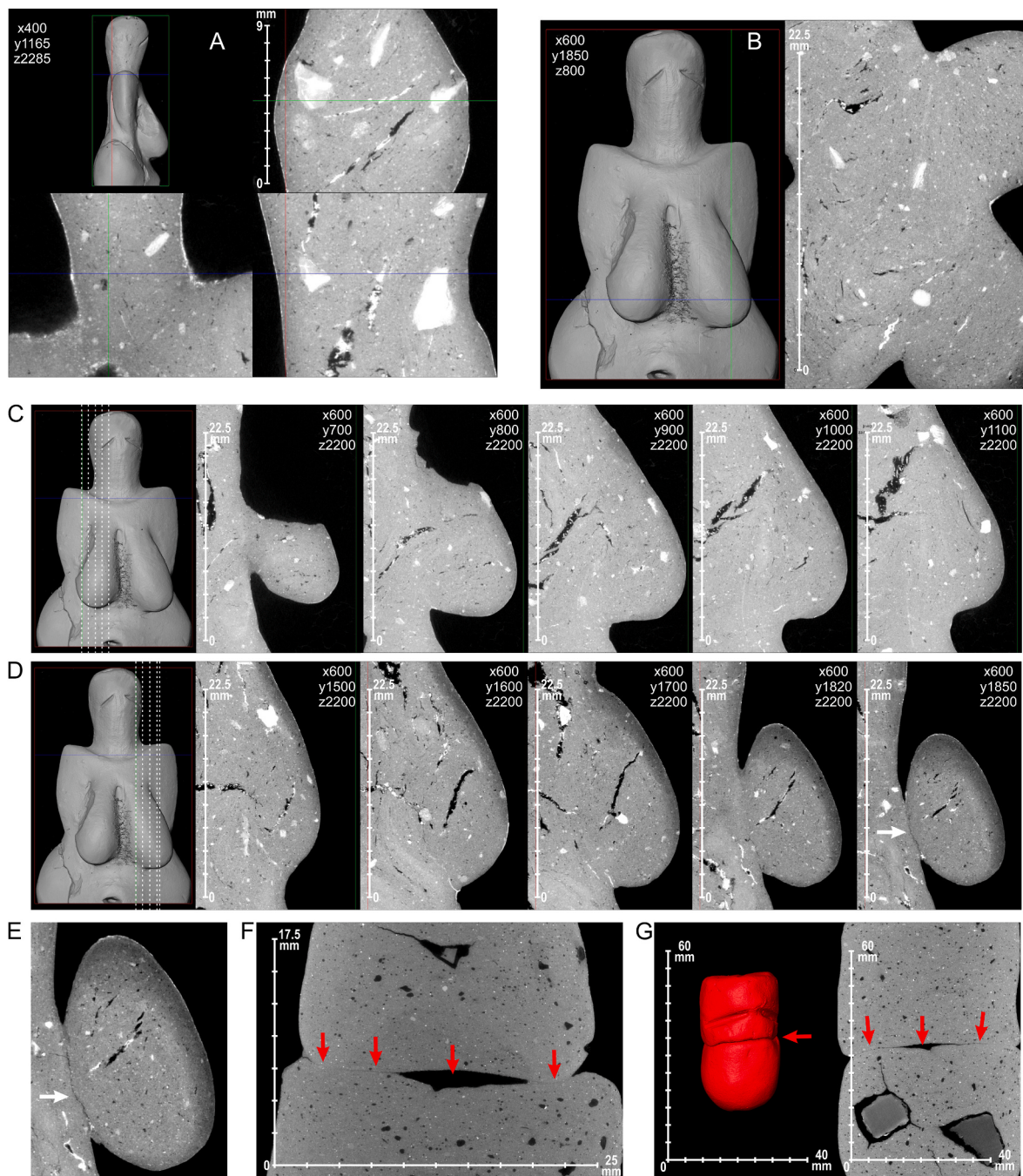


**Fig. 6.** Analysis of the shaping technology of the Venus in areas where additive technology could be applied. A - sections in the neck area; B - transverse section in the area of the breasts and hips; C - longitudinal sections in the area of the right breast; D - longitudinal sections in the area of the right breast, the white arrow shows an interlayer region represented the crack (for detail see 5:E); E - detail of the irregular interlayer region (the white arrow) in the area of the left breast; F - detail of the connection of two parts of the reference phantom 2019/2, two parts connected by wet compression and twisting (red arrows indicate character of the interlayer region); G - connection on the reference sample 2019/5 - connection of two slightly dried parts (red arrows indicate character of the interlayer region).

Within these cracks, very light objects of an irregular shape resembling branched crystals appear (Fig. 10:A). These irregularly shaped objects have multiple sharp protrusions (Fig. 10:A and B), while the whole structure resembles sea corals.

Two boreholes drilled into the body from the area where the body is attached to the broken-off part of the right leg are also related to the taphonomy of the statuette. They are identical in shape and size, measuring approximately 3 mm in diameter (Fig. 10:C and E). The larger hole goes as deep as 8 mm and reaches an inclusion (Fig. 10:D, light grey oval indicated by white arrow), which was the probable source of the chemical data indicating the presence of ivory remnants reported by

Karel Absolon.

#### 4. Discussion

##### 4.1. Composition of ceramic paste

The main goal of this analysis was to confirm or disprove the presence of inclusions that could have been added to the ceramic paste for symbolic reasons. The Venus itself is considered to have a symbolic purpose. Therefore, we cannot exclude the possibility that some of the artefacts or products of nature might have been placed into the body

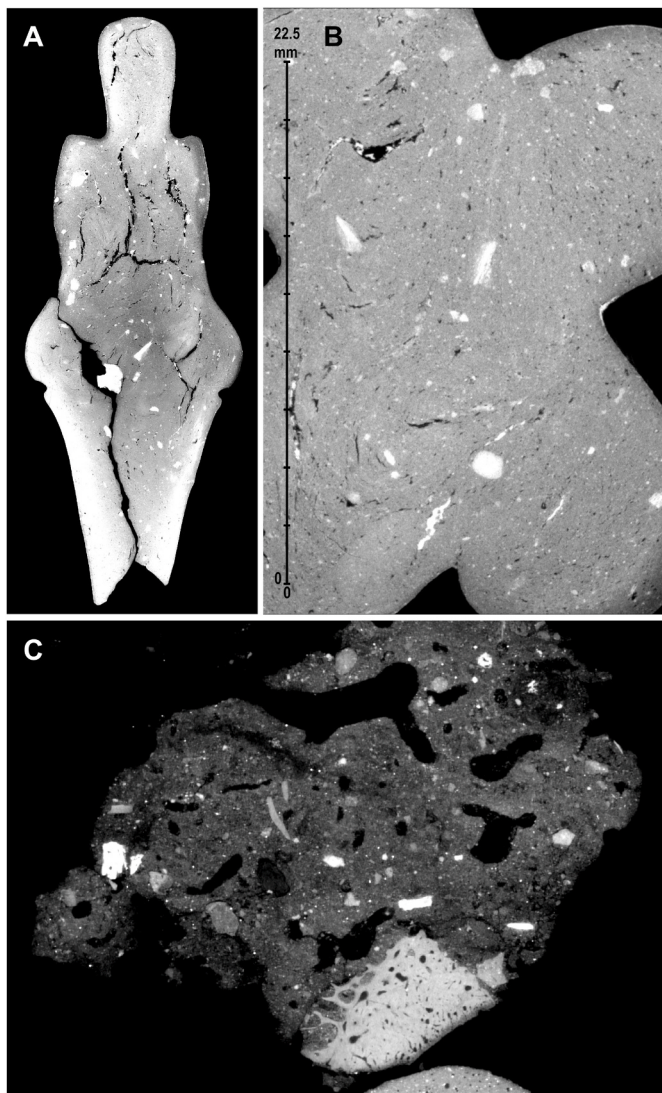


**Fig. 7.** Comparison of the porosity derived from  $\mu$ CT scans of the Venus (A – anterior view and B – superior view) and a lump of the original cultural layer from the Dolní Věstonice site (C). The ceramic paste of the Venus is more compressed in comparison to the original loess. Visualisation by P. Neruda.

intentionally. The material used – loess – provide us the space for such speculations because it is quite easy to add an object into the ceramic paste during the manufacturing process. This is proven, for example, by two Neolithic female statuettes from Malta (Rich, 2008).

The segmentation discovered a considerable number of inclusions in the clay material that were measured, and a group containing inclusions of a volume larger than  $2 \text{ mm}^3$  per inclusion which approximately matches the volume of a grain of rice, was set aside and subjected to further analysis. The particles of such size were quite easily manipulated by fingers; no known Gravettian symbolic or decorative artefacts are smaller than  $2 \text{ mm}^3$  (e.g. Lázničková-Galetová, 2022).

When considering materials that may have been included in the Venus statue for symbolic purposes, fragments of hard animal tissue from mammoths, such as bones and ivory, would be a likely choice. The mammoth played an important role in the everyday lives of Gravettian hunters and gatherers, and not only were these materials used to create objects of everyday use, but they also likely had a symbolic significance (e.g. Lázničková-Galetová, 2021; Lázničková-Galetová, 2022; Oliva, 2021; Svoboda, 2020; Wolf and Vercoutère, 2018). The high frequency of these types of findings might have influenced Absolon's interpretation of the results of chemical analysis, which should have indicated

mammoth bones and ivory as the predominant components for the building material of the statuette. Although such material remnants are quite easy to distinguish from other items on orthoslices, the data collected by CT scanning did not confirm the presence of any ivory or bones inside the Venus. We can, with high probability, rule out the original theory proposed by Absolon (1938b) and support the interpretation of the chemical makeup of the ceramic paste published by Vandiver (Vandiver et al., 1989).

Another material that might have had a symbolic significance and was significantly represented in the Gravettian culture was different types of mostly Tertiary mollusc fossils, such as those belonging to the *Dentalium* or *Melanopsis* genera (Cârciumaru et al., 2019; Hladilová, 2011; Soffer and Vandiver, 2005). In all cases, these are fossils of several centimetres in size. In the case of the Venus, the situation is somewhat different. The high resolution of the CT images made it possible to segment the fossils into 3D objects so that some of them could be taxonomically classified, similar to the case of the study of the Venus of Willendorf II limestone (Weber et al., 2022). We distinguished a few remnants of fossils that belonged to the Crinoidea class, usually in the shape of regular stars (Appendix B; Fig. 7:P29 and P39), or the Gastropoda class (Appendix B; Fig. 7:P29 and P39). The dimensions of the fossils do not exceed 3 mm in diameter, therefore it is highly unlikely that the remnants of these fossils were placed inside the body of the Venus intentionally. They are randomly distributed throughout the body of the figurine, with no special focus on a certain place, e.g. the head or the abdomen. Moreover, such microfossils could appear in loess as the result of contamination from Jurassic bedrock deposits caused by a variety of diluvial and deluvio-elolian processes. Such layers are commonly preserved at Dolní Věstonice I (Houša et al., 1963; Jüttner, 1922; Klíma, 1963, 1981; Svoboda et al., 2018). Due to these processes, small pieces of weathered Jurassic rocks commonly occur in overlaying layers that are rich in loess. If this type of loess were used as the main component of the ceramic paste (e.g. for creating the figurine), it would naturally lead to the presence of fossil remnants that commonly appear among the coarse pieces of Jurassic sediments.

The analysis of smaller inclusions with a volume of less than  $2 \text{ mm}^3$  did not provide any useful information about the use of these inclusions as the temper. We were looking for a specific group of inclusions that would be imported from different places, such as quartz grains with a high spherical index. In addition, we were looking for any clusters of these grains that could be caused by adding the temper to the paste or insufficient mixing of the ceramic paste. The statistical analysis did not prove any of these theories. The distribution of the inclusions was random. The higher level of sphericity that distinguishes a certain group of inclusions consisted solely of bright white inclusions, resembling crystals on the 3D model (Fig. 5:BS1; Appendix B; Fig. 9). Given their size, the occurrence inside the ceramic paste seems to be of natural origin. Considering their high density, we are most likely dealing with heavy minerals of some kind. These are a common component of elolian sediments. Similar objects in ceramics from the Hamburg-Boberg site are interpreted in the same way (Kahl and Ramminger, 2012). Our interpretation of the obtained results is that no temper was intentionally added to the ceramic mass during its preparation, and, on the other hand, the mass was not purified by releasing coarser impurities. This fully coincides with the published results of  $\mu$ -CT scans of Pavlovian ceramic pellets from DV I (Farbstein and Davies, 2017).

#### 4.2. The provenance of the sediment in the ceramic paste

Despite rather negative results, the gained insights can be used to improve our provenience knowledge of the sediments utilised in the ceramic paste by combining our information about the composition of the paste and the taphonomy analysis. The used sediment was calcareous, which is illustrated by the presence of  $\text{CaCO}_3$  nodules (Fig. 5:P47) and secondarily formed structures inside the cracks located in the inner part of the statuette. Calcareous sediments are represented by loess in

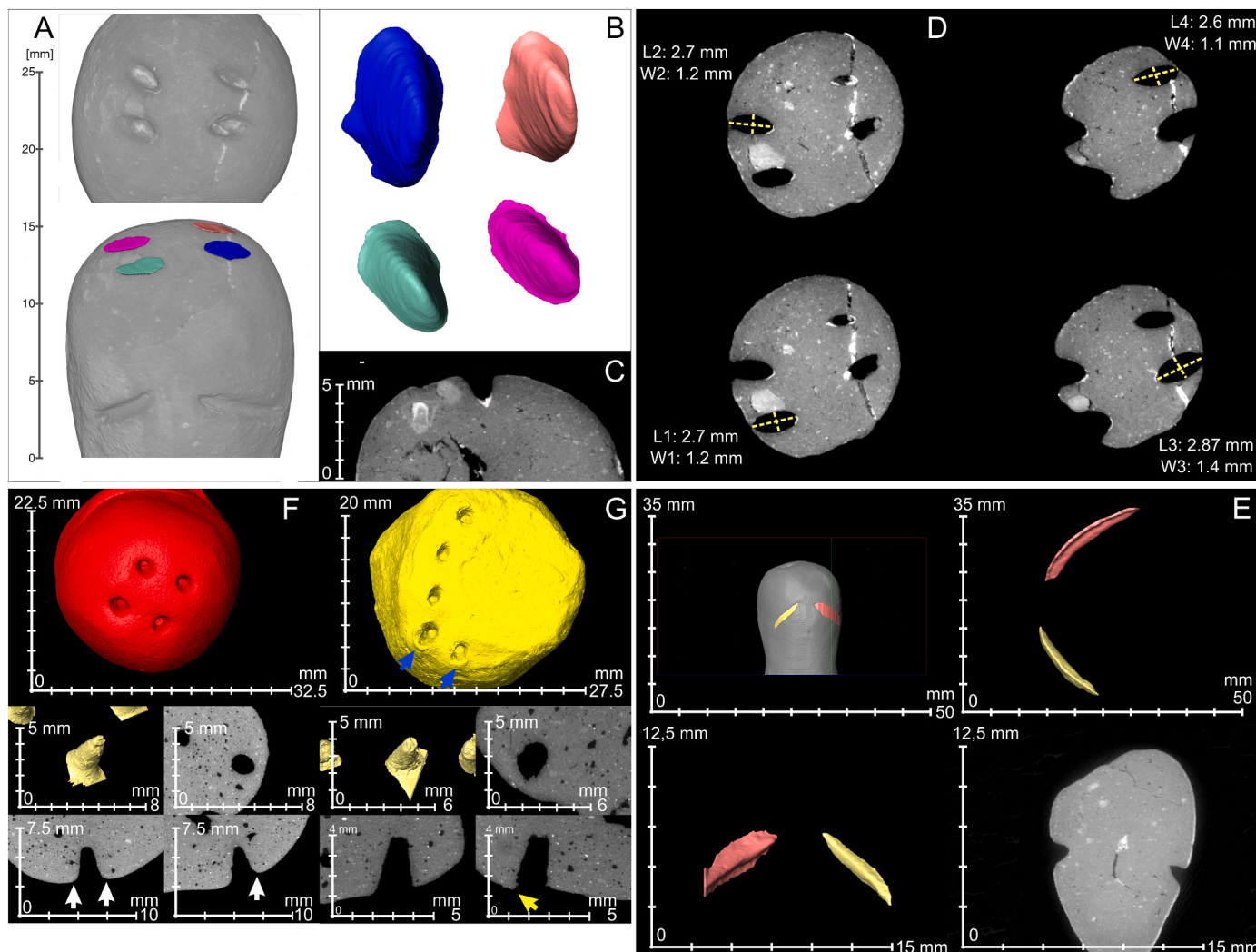


**Fig. 8.** Analysis of the punctures located on the top of the head and their comparison to the reference samples. A – position of 4 holes on the top of the head of the Venus head; B – segmented 2D model, cf. colours on A; a cross-section through one hole, the white matrix is carbonate; D – dimension of individual holes; E – morphology of eyes created in semi-dry ceramic paste; F –reference samples (Phantom 5) with holes made by a small pigeon feather to a semi-dry ceramic paste, borders of holes are rounded (see white arrows), similar to B; G –reference samples (Phantom 5) with holes made by a small pigeon feather to a wet ceramic paste, the shape of 3D imprints differs from imprints of original holes on the Venus's head (B) - borders of holes in cross-section create are sharp and the ceramic paste is pulled out into the small ridge (blue and white arrows). Segmentation and visualisation by P. Neruda.

the area of Dolní Věstonice. Even the presence of heavy minerals, which are a common part of loess, would not deviate from such a classification (Britannica, August 13, 2010). The original loess *in situ* is a clastic, predominantly silt-size sediment without any rock components. The only coarse components of a loess sediment are the CaCO<sub>3</sub> concretions. In the case of the Venus's ceramic paste, we recognised inclusions, mostly among inclusions larger than 2 mm<sup>3</sup>, that represent different rocks and Jurassic microfossils. It most likely means that the calcareous sediment is a type of loess contaminated by other sediments. If we refer to the cultural layer in Dolní Věstonice, we can find a loess-based sediment contaminated by sediments of Tertiary age and weathered Jurassic bedrock. The outlined interpretation does not contradict the results of an earlier chemical analysis of a ceramic fragment from the body of the Venus (Vandiver et al., 1989). Therefore, we assume that the main sediment for the ceramic paste was taken from the archaeological site area. However, the absence of hard animal tissue fragments and stone artefacts, which are typically found within a cultural layer, suggests that the material used to make the Venus was selected from an area outside the main living areas. It would have to be an area where the loess was contaminated by subsurface sediments, similar to the situation on the

archaeological site. Farbstein and Davies proposed that the building sediment was a naturally wet sediment found along the river Dyje (Farbstein and Davies, 2017). We cannot reject this theory; nonetheless, it is necessary to point out that a wet sediment could have been found even within the area of the site, for example, in puddles or depressions in the ground. Such places could be represented in Dolní Věstonice I by the watery terrain groove, on the western edge of which there was a deposit of mammoth bones. This place is about 20 m away from the spot where the Venus was found (Fig. 1:D). In this area, the contaminated loess sediments were well documented (Klíma, 1963; Novák et al., 2023). Moreover, the water could have added to the sediment intentionally (Vandiver et al., 1989).

#### 4.3. Chaînes opératoires remarks

The new µ-CT images can have a significant impact on the ongoing discussion about the questions related to the technological process used to produce the figurine. Given that it was not previously possible to examine the internal structures of the Venus in detail, there are certain debates regarding the technological process used to create it, specifically

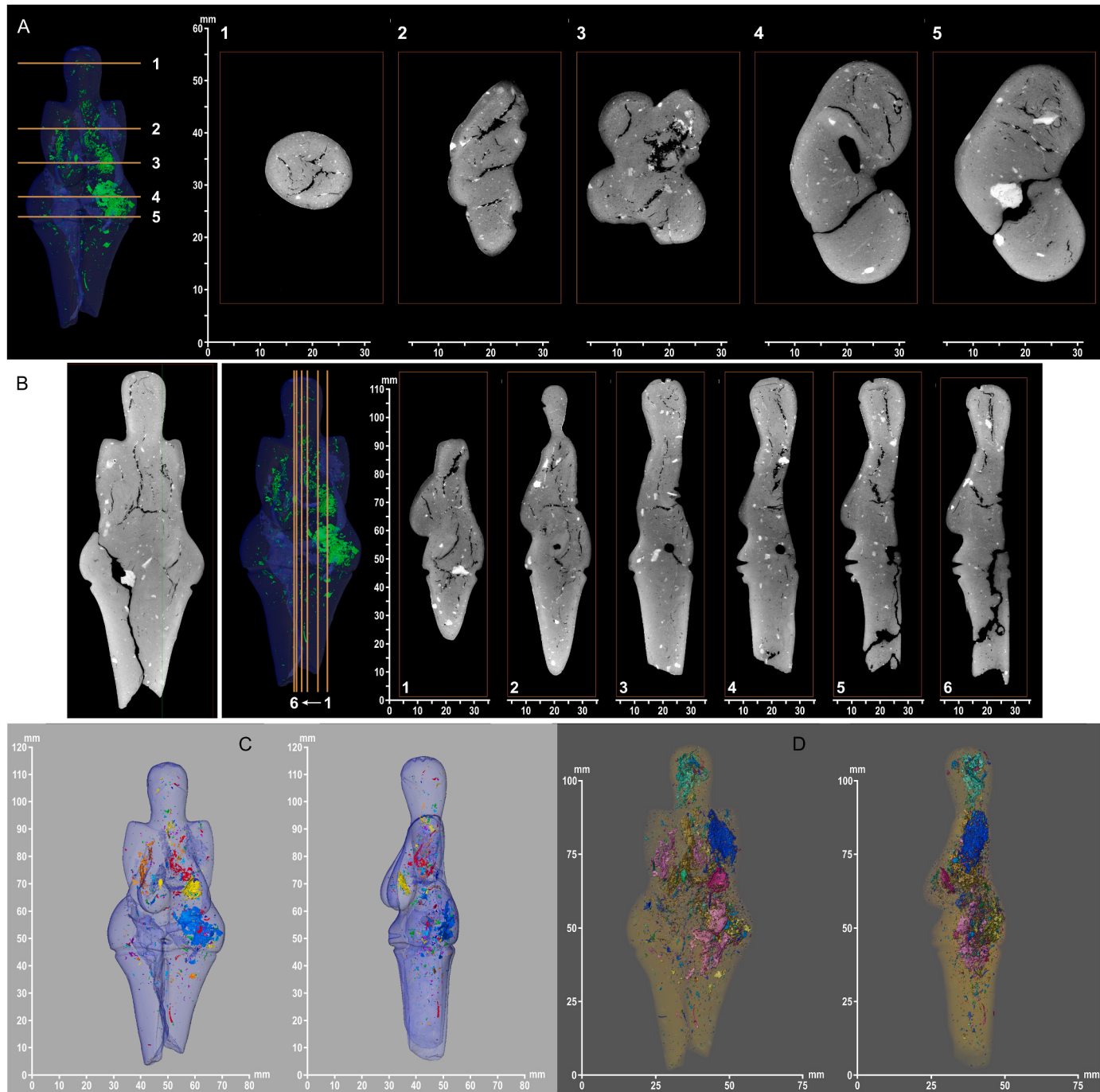


**Fig. 9.** Cracks and cavities inside the body of the Venus in cross-sections (A) and longitudinal sections (B). C - position and size of cracks that are not connected to the surface, D - position and size of all cracks. The cracks were formed during the firing process of the artefact. Segmentation and Visualisation by P. Neruda.

whether an additive method (Vandiver et al., 1989), a non-additive method (Farbstein and Davies, 2017), or a combination of both methods were used (Bougard, 2011; Farbstein and Davies, 2017; Gonyševová, 1999). Regarding the Venus itself, it seems easier not to have shaped the statue as a single piece, including the head and breasts, but rather to have fashioned them separately and then joined them together, possibly using organic tools. Alternatively, additional material could have been added to the specific parts of the core form in order to attach any protruding details of the body. The use of additive techniques in the process of making post-Palaeolithic figurines has been confirmed in various instances by applying microtomography (Kreiter et al., 2014; Pavel et al., 2013; Pizzeghello et al., 2015). Moreover, the additive

approach is indicated by multiple examples, including a broken-off breast fragment from the middle part of the archaeological site (Fig. 1:D and Fig. 11:D), other detached pieces of the body (Fig. 11:C, E, and F), broken heads (Fig. 11:A and B), and the lower part of legs (Fig. 11:G and H).

Nevertheless, a shrinkage gap between joined regions is usually visible (Kreiter, 2008) and is considered radiological evidence for slab-built vessels (Berg and Ambers, 2016). Such joins are used for the reconstruction of technological processes used for making Neolithic hand-made pottery (Kozatsas et al., 2018). Experimentally made phantoms also show joins between construction units (see Fig. 6:F and G). Only through the use of wet clays and the application of strong forces

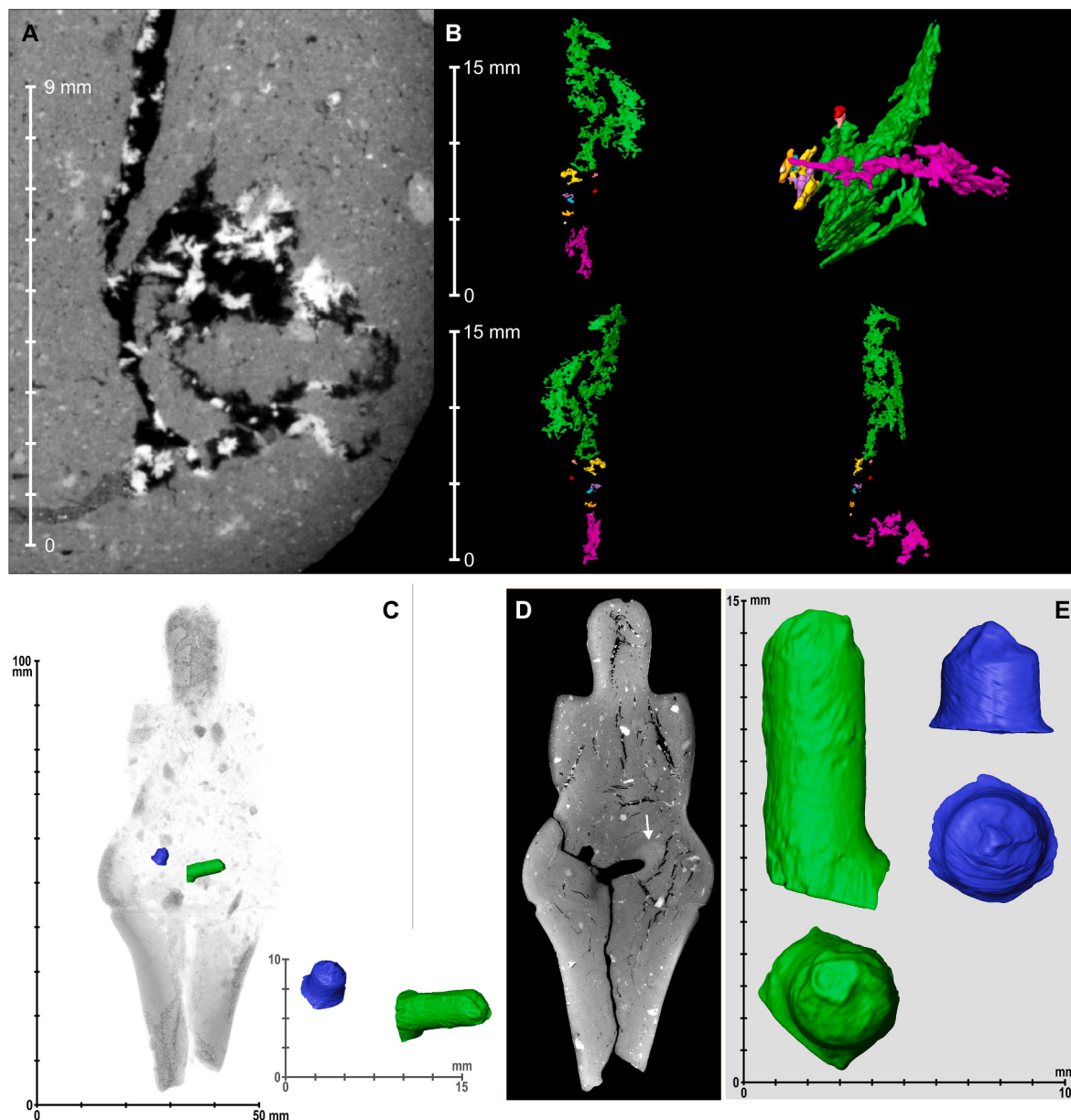


**Fig. 10.** Structures inside the cracks and two drilled holes. A – orthoViews of the growths in the cracks in the head area, B - segmented 3D models of growth structures that represent CaCO<sub>3</sub>-based crystals. C and D – position and E – the shape of probes drilled into the body of the Venus, probably under the curation of Karel Absolon. The white arrow indicates an inclusion that could serve as the source of data for Absolon. Segmentation and visualisation by P. Neruda.

that cause homogenising adhesion can traces of joins among individual construction units be thoroughly eliminated (Kozatsas et al., 2018). Such conditions are difficult to fulfil in the case of figurines because the application of strong force in one direction affects the shape of the figurine on the opposite side.

The analysis of radial, horizontal, and tangential sections did not uncover any joined regions among possible individual parts of the Venus. The one join area is visible only on the outer part of the left breast and has an irregular shape that corresponds with the micromorphology of the rough dry join type (for definition see Kozatsas et al., 2018). It was most likely created by pressing a piece of semi-dry material of the breast towards the body during the shaping of this part. All this suggests that the creator used a non-additive method. There are a few more instances of the use of the non-additive method across the area inhabited by the Pavlovian people, as noted by Farbstein and Davies (2017).

Additionally, the experimental phantoms revealed that the final details on the surface, such as the legs, navel, eyes, and punctures on the

head, were made on partially dried ceramic material by using a pointed tool. Thus, the results correspond with the previously published analysis of animal figures found in Dolní Věstonice (Farbstein and Davies, 2017).

It would be useful to compare different techniques for the preparation of ceramic paste, particularly in comparison with other experimental figurines. It could be interesting, for example, to compare the porosity of several Palaeolithic statuettes, possibly original pieces and copies made experimentally, using different methods according to methodological procedures developed for studying historical bricks (Reedy and Reedy, 2022a). Our data suggests that the statuette was shaped from a piece of ceramic pasted moulded into some kind of cylindrical form. This is indicated by the vertical distribution of the main cracks in the material (Fig. 9), a certain directing of pores and inclusions into layers following the shape of the Venus in cross-section (Fig. 7A and B). From the technological processes of ceramic moulding, this would correspond to the so-called pinching (Berg and Ambers, 2016) or moulding (Kozatsas et al., 2018; Middleton, 2005) techniques, although

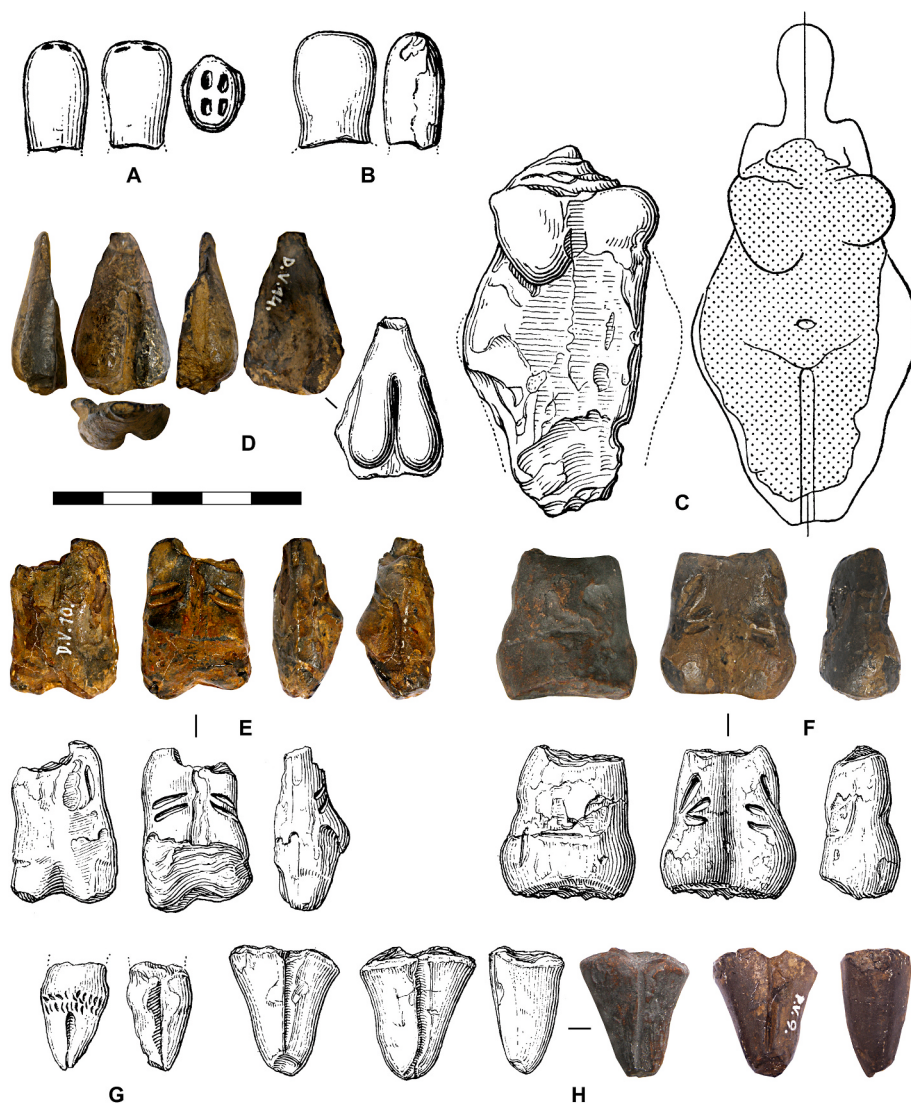


**Fig. 11.** Fragments of other finds of Venus found at the Dolní Věstonice site. A–B heads, C fragment of a body, D fragment of breasts, E–F fragments of middle parts of Venus, G–H fragments of legs. A–C and G the collection of the Archaeological Institute of the Czech Academy of Sciences; D–F and H the collection of the Anthropos Institute of Moravian Museum. Drawings A–D according to Klíma (1983), E–H Klíma (1981) and photos D, E, F and H made by J. Cága (archive of the Moravian Museum).

the terminology created to describe the production of vessels is difficult to apply to figurative plastic art.

An interesting question arises regarding the level of ceramic technology in the Gravettian period. According to Bougard (2011), the process of ceramic use was standardised, allowing for the transfer of manufacturing information from generation to generation in a consistent form. This theory is supported by multiple findings of statuettes from Dolní Věstonice I, II, and Pavlov I. However, this resemblance does not provide any information about how the ceramic material was processed and fired. Considering the technology, Farbstein and Davies previously pointed out, based on the results of  $\mu$ -CT images of animal figurines, the experimental character of this new technology in the Palaeolithic (Farbstein and Davies, 2017). This conclusion can be supported by the results of this analysis. The character of the ceramic paste suggests the presence of non-standardised coarse inclusions that have affected the homogeneity of the paste and the result of the firing process. The cracks and fractures visible on the figurine were not the result of deliberate manipulation, as was the case with some animal Palaeolithic figurines (Soffer and Vandiver, 1994).

#### 4.4. Taphonomy and its implication for future protection

The scans revealed frequent cracks inside the body of the Venus, some of which are not connected to the surface. There are two main issues arising from this discovery.

Firstly, the cracks reduce the homogeneity of the material, increasing the impact resistance, mainly in the area of the abdomen or head. The second issue is related to the enclosed cavities, which can lead to structural destabilisation caused by a rapid drop in atmospheric pressure. This can be especially challenging while transporting the figurine.

It is highly unlikely that the missing part of the lower limbs will ever be found. Nevertheless, it is worth noting that their original shape was pointed, as we can illustrate in examples of similar figurine fragments found in Dolní Věstonice (Fig. 11:G and H).

#### 4.5. Methodological remarks for $\mu$ CT scanning and image processing

For the scan of the statue itself, we chose a helical (spiral) trajectory and acquisition scheme, which is suitable for iterative data reconstruction. Thanks to the helical trajectory, we were able to scan more than half of the statuette's volume in one pass. Thus, two scans were enough

for the entire acquisition of the statuette, including the phantoms. If we were to use a more traditional circular scan, there would be up to 6 scans that would require stitching together. The data would thus be more significantly disturbed by the so-called stitching artefact, which would reduce the accuracy of later data analysis (Kalender, 2011).

Using the helical trajectory, the sample moves in two axes during the scan – rotational and translational, which makes it more difficult to maintain the exact positions of the acquisition scheme, especially if we want to achieve resolution in the order of micrometres. However, an algorithm can be used to reconstruct the data. This can compensate for the mechanical inaccuracy of the sample movement during scanning and thus achieve a perfect scan trajectory (Varslot et al., 2011).

A significant problem was identified within the statistical processing of the original data set. The exploratory analysis of the original dataset discovered erroneous records (corrupted data) that represent approximately 5%–10% of all records, depending on the feature being examined. These records included faulty values in relation to their physical characteristics, such as an elongation value of -1, which is beyond the possible range between 0 and 1. Similar problems appeared in the context of other features, such as anisotropy or flatness. It is crucial to point out that all of these erroneous values had a minuscule volume with a maximum volume of 0.000034 mm<sup>3</sup> and an average volume of 0.000009 mm<sup>3</sup>.

#### 4.6. Gravettian ceramic production

Despite the relatively lower level of technological advancement in

ceramic production during the Gravettian period compared to later prehistoric periods, it was a cultural practice firmly rooted in the Gravettian population in much of Central Europe and the Central Danube region (Fig. 12). Based on the discovery of various forms of figurative art in complete or fragmentary form, the centre of Gravettian ceramic technology is believed to have been located near the Pavlov Hills in Moravia. However, it is important to note that the Dolní Věstonice I (Bougard, 2011; Oliva, 2015; Svoboda, 2020) and Pavlov I (Bougard, 2011; Farbstein and Davies, 2015; García Diez, 2005; Svoboda, 2020) sites, both located in the area, are the only sites that have provided rich collections of largely preserved human and animal statuettes. Other findings from sites such as Pavlov VI (Svoboda et al., 2009) or Krems-Wachtberg (Einwögerer and Simon, 2008; Händel et al., 2009) only consist of pieces of animal statuettes, while findings from Pavlov II, Borskice-Chrástka, Dolní Věstonice II, and Přerov-Předmostí are only oval-shaped or conically-shaped clods of ceramic material that cannot be classified as figurative art (Bougard, 2011; Gonyševová, 1999; Králík et al., 2008; Soffer and Vandiver, 1994, 1997, 2005). Nevertheless, most of these fragments have an irregular shape, making it difficult to determine whether they are associated with ceramic production or are just a by-product of any human-conducted firing process. When looking at regions outside of Central Europe and the Danube area, there are other sites with animal figurative art discoveries, for example, Vela Spila in Croatia (Farbstein et al., 2012) which belongs to the Epigravettian culture, or ceramic fragments from Kostenki (Zheltova and Yanshina, 2015).

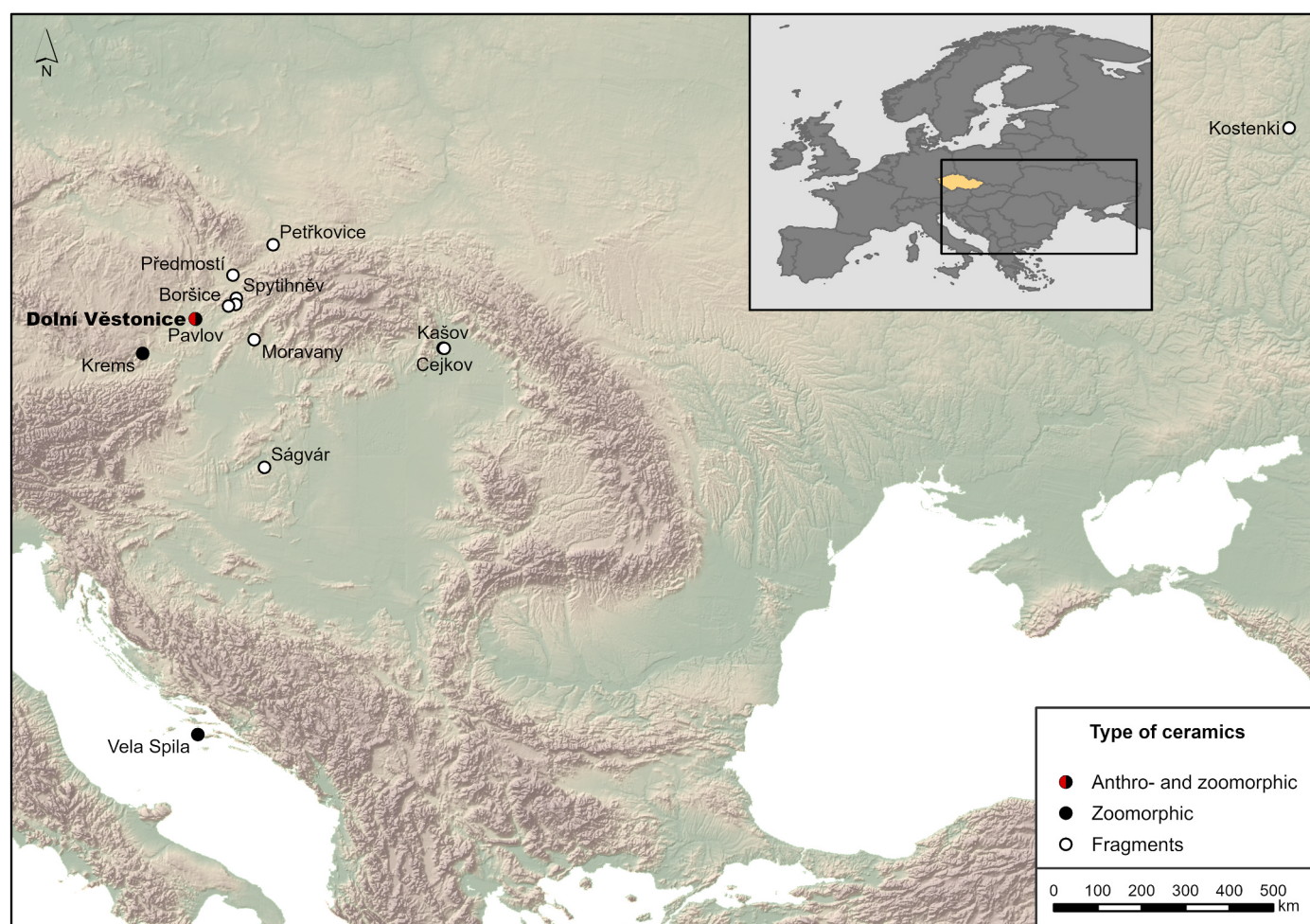


**Fig. 12.** Map of the distribution of burnt clay in Europe. The yellow colour in the map (upper) indicates the position of the Czech Republic. Map P. Neruda, using SRTM90mDEMver4 (Jarvis et al., 2008).

## 5. Conclusion

$\mu$ -CT scanning of the Venus of Dolní Věstonice provided high-resolution images that enabled the study of the inner structure in detail. By studying orthoslices and segmented 3D models, we confirmed that the Venus was made of a loess-based sediment with a natural admixture of Jurassic rocks derived from the bedrock. This finding aligns with the composition of the cultural layer in Dolní Věstonice. Several fragments of Jurassic microfossils were identified inside the figurine's body. However, Karel Absolon's conjecture regarding possible fragments of mammoth tusks and bones inside the building material of the Venus was disproved. A similar outcome applies to the theory of the possible symbolic placement of small objects inside the body. In addition to this, the spatial distribution of small rock particles does not indicate any intentional manipulation of the content of the building material in this sense, since the distribution is random and without any visible clusters. On the other hand, the analysis showed interesting results regarding the technique of forming the statuette, where a so-called non-additive technique seems to be the most likely procedure chosen by the creator. Subsequently, we can assert that indented elements such as four holes, eyes, and a navel on the surface were pushed into the semi-dry ceramic material. The discovery of fairly frequent internal cracks represent another interesting finding from the point of view of taphonomy. Under certain conditions, these could cause the disintegration of the statuette, which must be taken into consideration while manipulating the Venus.

### Competing interest declaration

The authors declare no competing interests.

### Additional information

The original data are stored in the Moravian Museum and Thermo

Fisher Scientific (both Brno, Czech Republic). Statistical analyses are available on [GitHub](#). The authors declare no competing financial interests. Readers are welcome to comment on the online version of the paper.

### CRediT authorship contribution statement

**Petr Neruda:** Writing – review & editing, Writing – original draft, Visualization, Investigation, Conceptualization. **Petr Hamrozi:** Writing – original draft, Formal analysis. **Zuzana Patáková:** Writing – original draft, Resources, Project administration. **Grzegorz Pyka:** Resources, Data curation. **František Zelenka:** Writing – original draft, Resources, Data curation. **Šárka Hladilová:** Writing – original draft, Investigation. **Martin Oliva:** Writing – review & editing, Writing – original draft. **Eva Orságová:** Visualization.

### Declaration of competing interest

The authors declare that they have no known competing financial interests or personal relationships that could have appeared to influence the work reported in this paper.

### Acknowledgements

This paper was financially supported by the Ministry of Culture of the Czech Republic through institutional financing of the long-term conceptual development of the research institution (the Moravian Museum, MK000094862) for the years 2024–2028. We would like to thank Sebastian Pfeifer from Friedrich-Schiller-University in Jena (Germany) who provided small fragments of fresh ivory. We would like to also acknowledge the efforts of the police of the Czech Republic for providing protection during the transport and scanning of the Venus. We express gratitude to the laboratory of the Archaeological Institute of the Moravian Museum for the burning of reference samples.

## Appendix A. – Statistical analysis

### 1. Exploratory analysis

Original dataset for the statistical analysis was generated by the Avizo software in Standard Shape Analysis format, which consisted of 102,515 records and 37 different features (see [original dataset](#)).

During the exploratory analysis of the original dataset, a huge percentage of erroneous records were discovered, representing approximately 5%–10% of all records depending on the feature being examined. These records included faulty values in relation to their physical characteristics, such as the elongation value of -1, which is beyond the possible range between 0 and 1. Similar problems appeared in the context of other features, such as anisotropy or flatness. It is crucial to point out that all of these erroneous values had a minuscule volume with a maximum volume of 0.000034 mm<sup>3</sup> and an average volume of 0.000009 mm<sup>3</sup>.

To prevent any misleading results, all erroneous records were removed from the subsequent analysis. In addition to the invalid values that were identified, other outliers were detected with values that were extremely close to 0 or 0.99 for anisotropy, elongation, and flatness. Although these values do fall within the acceptable range for these parameters. As none of these outliers appeared in the group of particles that had a volume of 2 mm<sup>3</sup> or greater, their thorough analysis was deemed unnecessary for the scope of this study.

Furthermore, there were over 10 unnecessary features (such as eigenvectors and eigenvalues) generated automatically by the software AVIZO for processing the CT images that were not required for our analysis. All these features were as well not utilised in subsequent analyses. In total, eight features were used from the original data file including all particle coordinates (barycenter x, barycenter y, barycenter z), volume, voxel face area, anisotropy, elongation, and flatness ([Tables 1 and 2](#), and [preprocessed data](#)).

**Table 1**

Summary statistics of the entire cleaned dataset.

Statistics	Features					
	Volume [mm <sup>3</sup> ]	Anisotropy	Elongation	Flatness	VoxelFaceArea [mm <sup>2</sup> ]	Sphericity
<b>count</b>	92320	92320	92320	92320	92320	92320
<b>mean</b>	0.010785	0.746096	0.539786	0.474873	0.162819	0.643407
<b>std</b>	0.380968	0.182282	0.230214	0.265469	1.725816	0.070223
<b>min</b>	1.36E-05	0.000357	1.20E-21	0	0.003584	0.167262

(continued on next page)

**Table 1** (continued)

Statistics	Features					
	Volume [mm <sup>3</sup> ]	Anisotropy	Elongation	Flatness	VoxelFaceArea [mm <sup>2</sup> ]	Sphericity
25%	7.47E-05	0.628122	0.361577	0.278658	0.012904	0.608038
50%	0.00021	0.771202	0.535856	0.489836	0.026525	0.650886
75%	0.000733	0.890259	0.713814	0.678028	0.063803	0.68979
max	91.7529	1	0.99998	1	244.736	0.805996

**Table 2**Summary statistics of particles with a volume greater than or equal 2 mm<sup>3</sup>.

Statistics	Features					
	Volume [mm <sup>3</sup> ]	Anisotropy	Elongation	Flatness	VoxelFaceArea [mm <sup>2</sup> ]	Sphericity
count	69	69	69	69	69	69
mean	7.194427	0.749591	0.522337	0.490613	43.18686	0.399711
std	11.87967	0.138979	0.190592	0.223466	40.25292	0.082241
min	2.05733	0.373645	0.141648	0.094506	15.814	0.222475
25%	2.64934	0.659225	0.399644	0.304423	22.9474	0.334487
50%	3.76338	0.762504	0.492984	0.491434	29.3879	0.406799
75%	7.21237	0.860182	0.672624	0.626743	44.7756	0.464705
max	91.7529	0.96651	0.917335	0.959761	244.736	0.557364

## 2. Descriptive statistic

Besides the features automatically generated by the AVIZO software, another feature so called sphericity was calculated. This feature is one of the most useful ways to describe non-spherical objects, describing how closely the shape of a measured object approaches the sphere shape. It is conveyed as a value between 0 and 1. To calculate the sphericity of a particle the surface area ( $A_p$ ) and the volume ( $V_p$ ) were used Wadell's sphericity factor (Wadell, 1932), defined as:  $\psi = (\pi^2 / 3) (6V_p)^{2/3} / A_p$ , where  $A_p$  is the area of a particle and  $V_p$  is the volume of a particle (see [sphericity](#)).

The entire cleaned dataset was at first examined as a whole, however, due to a significant overlap caused by the sheer number of particles, a hypothetical boundary was set under the assumption that smaller particles, could not have been deliberately added to the building material of the Venus for any intended purpose. The boundary was established based on a particle volume of two cubic millimetres, which is roughly equivalent to the size of a small grain of rice. This distinction is significant from the perspective of exploring the intentional addition of distinct particles into the ceramic paste, mostly for symbolic purposes. To investigate this hypothesis we decided to look for potential clusters of material within the body of Venus.

Initially, we decided to use a clustering technique for all scanned particles no matter what size. Secondly, a more doable approach was chosen by limiting the data input for an unsupervised algorithm only to records with a total volume of 2 mm<sup>3</sup> or more, totalling to 69 particles. Despite being a small subset, these particles constitute 49.9% of the overall volume of all particles obtained from the cleaned dataset. Clustering analysis was selected as the method to identify potential patterns in the dataset based on similarities in the feature values. In particular, K-means++ was utilised as the primary technique for pattern recognition due to its simplicity and efficiency. The WSS (within-cluster sum of squares) and silhouette score were used as the primary metrics to determine the optimal number of clusters (K). The crucial input parameters used for the clustering algorithm were the space coordinates (BaryCenters) of all scanned particles. After applying the elbow method with the WSS metric, 2 clusters were designated. The null hypothesis ( $H_0$ ) for this case was defined as there is no significant difference regarding the mean values of the physical measurements between the first and second clusters.

$$H_0 : \mu_1 - \mu_2 = 0$$

These measurements include anisotropy, elongation, flatness and sphericity. As the main statistical test, two-sample t-test was chosen, where the first cluster contains 37 particles and the second one 32. The p-values for all the differences between two samples for each feature were greater than 0.05, indicating that there was no significant difference between any of these samples.

Subsequently, we tried to group our particles based on their physical features including anisotropy, elongation, flatness and sphericity. Initially, a PCA analysis was conducted on standardised (z-score) features of particles with a volume of 2 mm<sup>3</sup> and more. Only two components were taken into consideration as they account for more than 80% of the total variance. The K-means++ algorithm was applied to the PCA scores obtained earlier. To determine the optimal number of clusters, the elbow method was employed and determined that three clusters would be the best choice. We then labelled our original data according to the resulting cluster designations and plotted it in a 3D scatterplot. The first two clusters exhibited overlap, whereas the third cluster formed a relatively homogenous group in the upper torso area of the Venus.

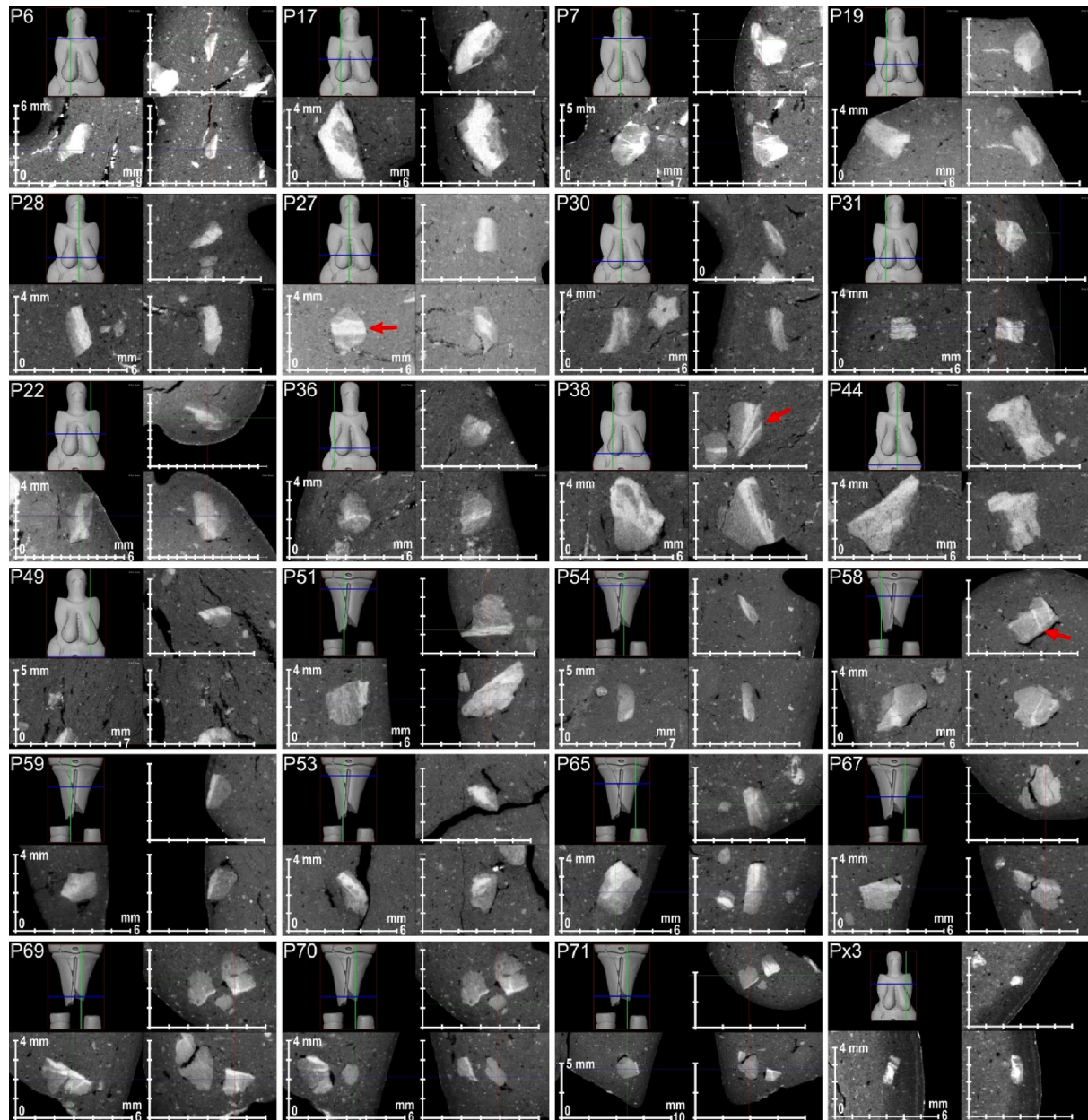
The distinctiveness of this particular cluster was indicated by its high average anisotropy value (0.880) and very low average flatness value (0.251). Although the original volume threshold only identified 69 particles, we chose to reduce the threshold from 2 mm<sup>3</sup> to 1 mm<sup>3</sup> in order to increase the number of particles in our analysis. By doing so, we were able to reduce the uncertainty of our results and increase the probability of correctly rejecting the null hypothesis.

The same procedure as for the particles greater than or equal to 2 mm<sup>3</sup> was applied to the particles with a volume greater than 1 mm<sup>3</sup>. The result clusters were far less distinct from each other from a physical perspective and their spatial distribution was rather evenly spaced without any distinct agglomerations across the figurine's body. Considering that the k-means algorithm belongs to so-called non-deterministic (stochastic) methods and the result interpretability and the performance evaluation are not as trivial as in the case of supervised learning algorithms.

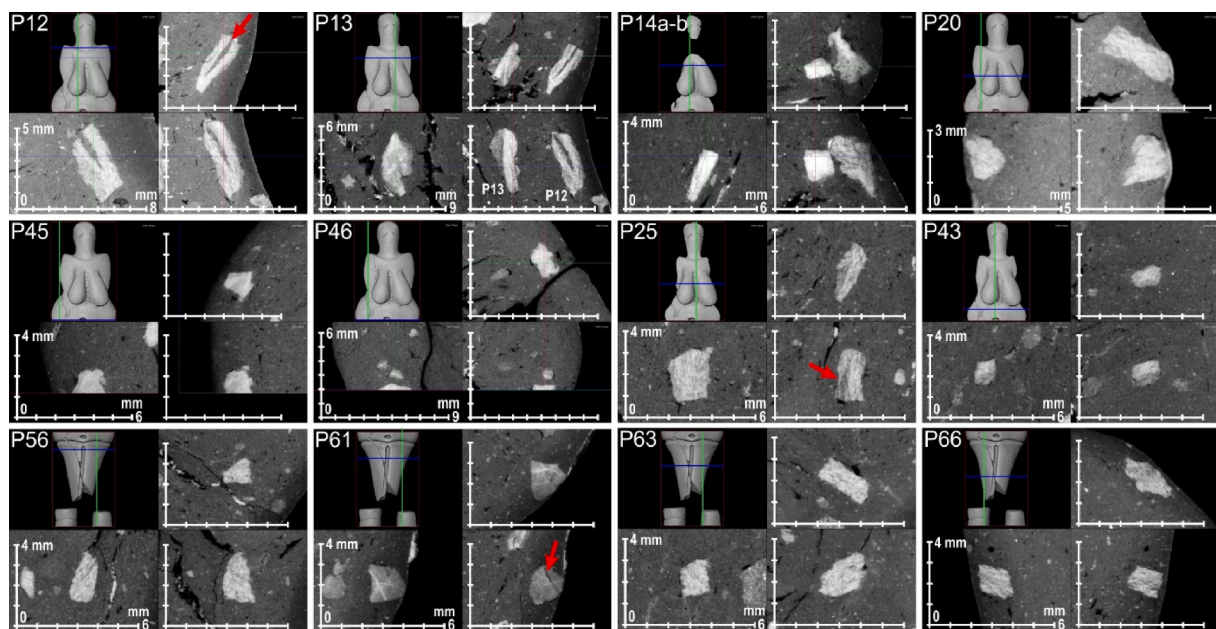
Our third approach to address the clustering problem involved dividing the figurine into six equal-sized parts along the vertical axis, using the

BarycenterZ coordinates. Particular attention was given again to the particles with a volume greater than or equal to  $2 \text{ mm}^3$ . The mean values of the physical features were found to be quite similar across all six parts, and the proportion of particles with a volume of  $2 \text{ mm}^3$  or greater in a given part of the Venus figurine ranged from 0.34% in the head part slice to 0.82% in the upper torso part slice. These proportions did not show any significant fluctuations (see, [clustering](#)).

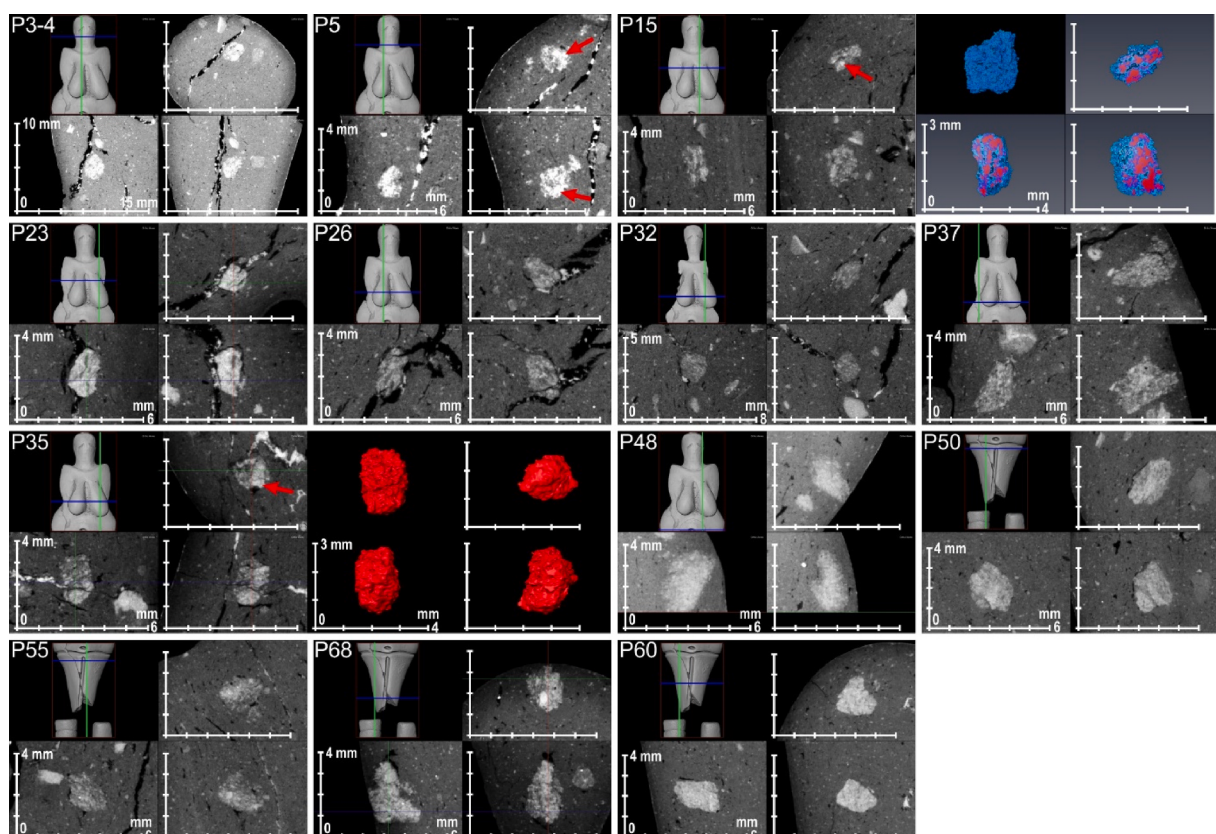
#### Appendix B. – description of inclusions $\geq 2 \text{ mm}^3$



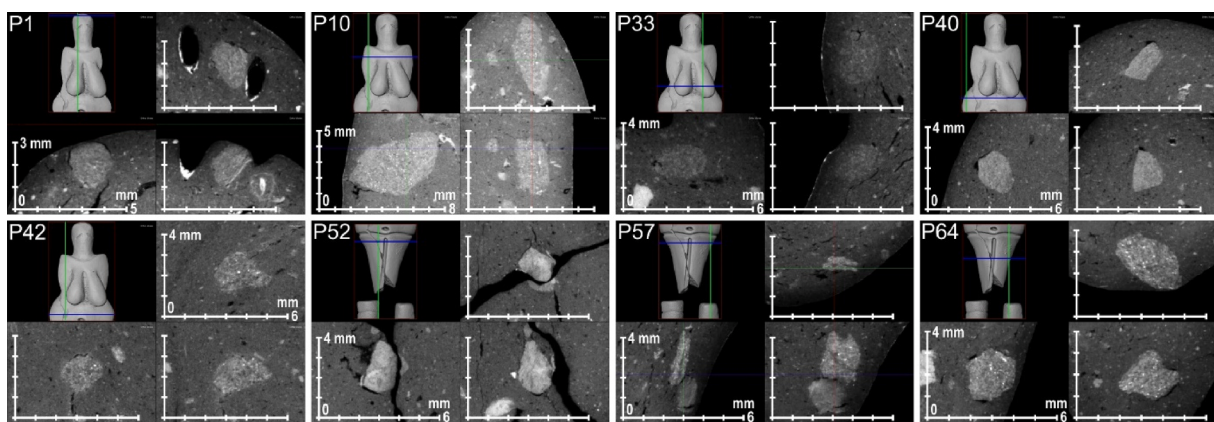
**Appendix B Fig. 1.** Catalogue of inclusions bigger than  $2 \text{ mm}^3$ . Group 1: Compact prism particles with slightly rounded edges and prominent veins running through them (some examples indicated by red arrows. Orthoviews: XY (right-top), XZ (right-bottom), YZ (left-bottom). Numbers correspond to particles in [Fig. 4:A](#).



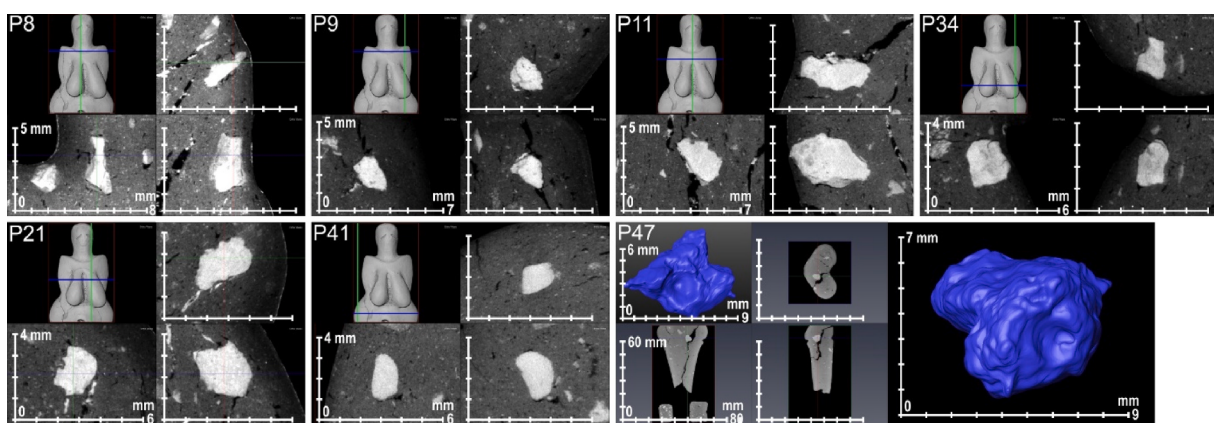
**Appendix B Fig. 2.** Catalogue of inclusions bigger than 2 mm<sup>3</sup>. Group 2: particles cf. Group 1 with disintegrated structures. Orthoviews: XY (right-top), XZ (right-bottom), YZ (left-bottom). Numbers correspond to particles in Fig. 4:A.



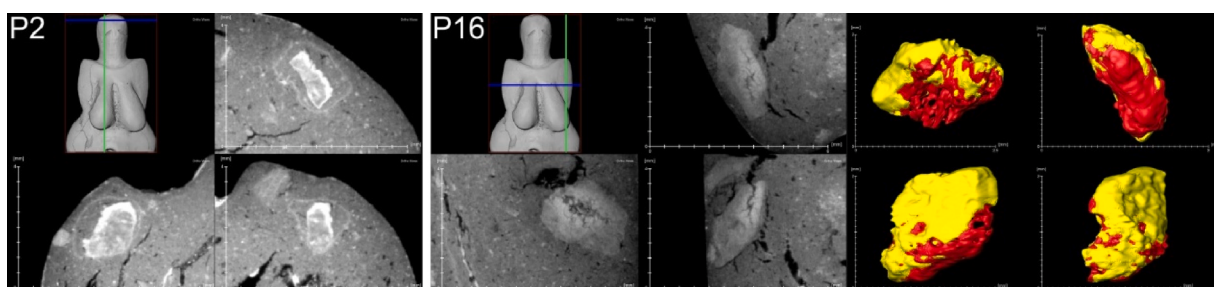
**Appendix B Fig. 3.** Catalogue of inclusions bigger than 2 mm<sup>3</sup>. Group 3: inclusions with disintegrated structures with higher density parts (the best example indicated by red arrows and blue and red parts of 3D model P15), slightly rounded edges and eroded surfaces (see 3D models in blue and red colours and blue). Orthoviews: XY (right-top), XZ (right-bottom), YZ (left-bottom). Numbers correspond to particles in Fig. 4:A.



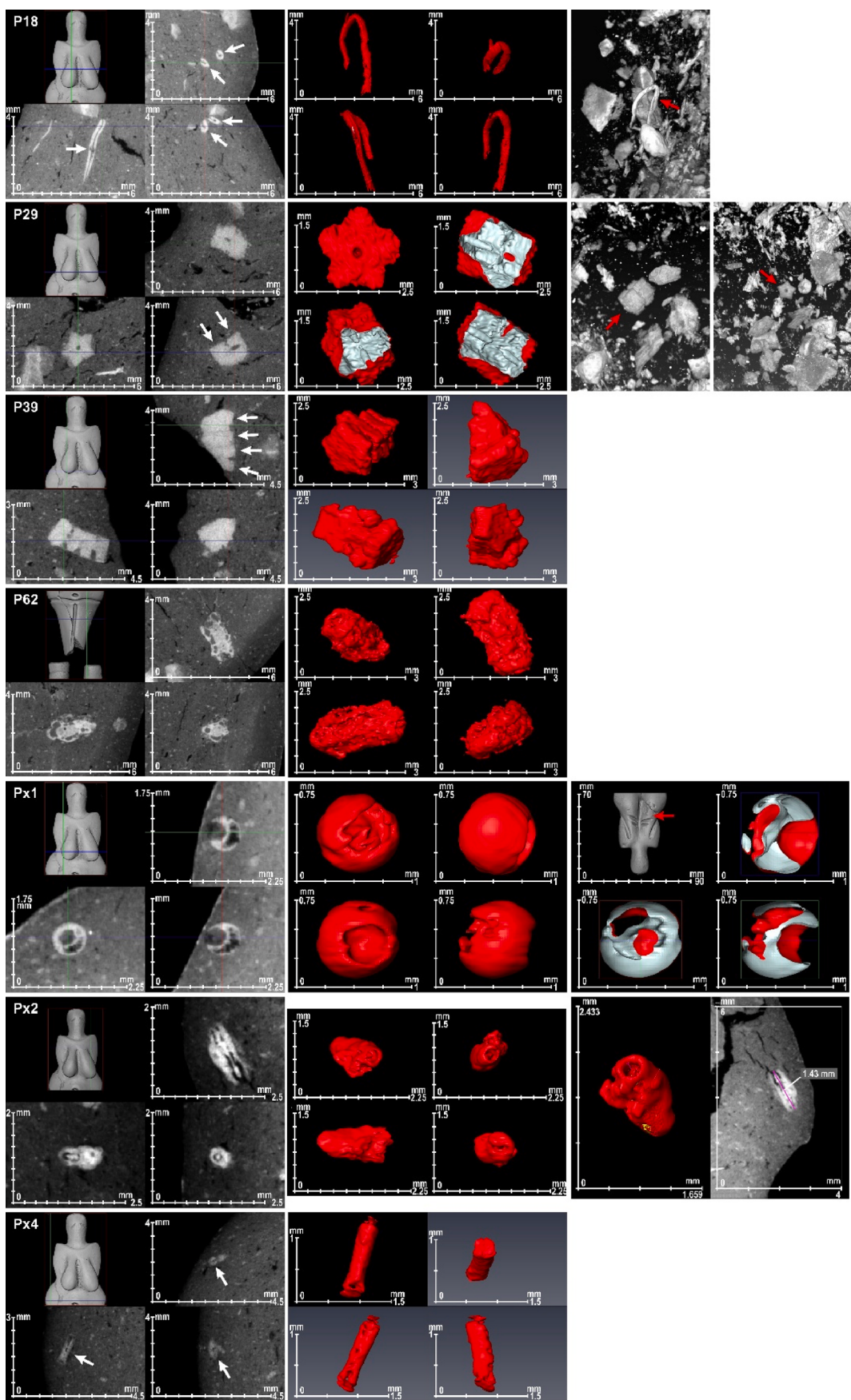
**Appendix B Fig. 4.** Catalogue of inclusions bigger than  $2 \text{ mm}^3$ . Group 4: inclusions with a slightly rounded shape and with a porphyritic inner texture. Orthoviews: XY (right-top), XZ (right-bottom), YZ (left-bottom). Numbers correspond to particles in Fig. 4:A.



**Appendix B Fig. 5.** Catalogue of inclusions bigger than  $2 \text{ mm}^3$ . Group 5: higher density particles, relatively homogenous, from irregular (cf. the blue 3D model P47) to rounded shapes (cf. the 3D model P41). Orthoviews: XY (right-top), XZ (right-bottom), YZ (left-bottom). Numbers correspond to particles in Fig. 4:A.



**Appendix B Fig. 6.** Catalogue of inclusions bigger than  $2 \text{ mm}^3$ . Group 6: oval particles with an irregular internal structure. Orthoviews: XY (right-top), XZ (right-bottom), YZ (left-bottom). Numbers correspond to particles in Fig. 4:A.



**Appendix B Fig. 7.** Catalogue of inclusions bigger than  $2\text{ mm}^3$ . Group 6: microfossils. White arrows indicate the position on orthoviews, red arrows the position of fossils among the surrounding particles (P18 and P29, right images) and in the body of Venus (Px1). 3D models segmented in red colour, view into objects – silver

parts. Orthoviews: XY (right-top), XZ (right-bottom), YZ (left-bottom). Images and models by P.N, classification by Š.H.

**P18. unidentified organic object**

Orthophoto (right side) – an object with a cylindrical shape that bends into a hook-like structure. It is approximately 7 mm in length and 0.2 mm in width.

The 3D image (in the middle, in red) indicates approx. circular cross-sectional view of the object, furthermore, there are at least 3 small holes of the same size, evenly spaced from each other and a continuous groove that extends throughout the object's entire length. There are structures similar to incremental lines, at one place, the outer layer of these structures is visibly peeling off.

Orthophoto (left side) – longitudinal section, cylindrical shape, an object is slightly bent with thick edges accounting for approx. 4/5 of the total diameter. There is a visible cavity stretching throughout the entire length (its diameter is approx. 1/5 of the whole). Transverse structures (segments) are not well visible in the image. Transverse cross-sections of approximately elliptical shape, with 'grooves' visible on their perimeters that reach up to "the central canal"?

P29

*class: Crinoidea indet. (sea-lilies), order: ?Isocrinida*

On the left side in orthophotos and the 3D model in the middle, two segments that are still connected (pluricolumnal) are visible (white arrows). The outlines of the crinoid columnals show a five-part radial symmetry and the hole in the centre of the columnal is a part of the so-called axial canal.

On the right side of the orthophotos, isolated segments of various types of crinoids are clearly visible. P29 indicated by red arrows.

P39

*class: Crinoidea indet. (sea-lilies), order: ?Isocrinida*

Both in orthophotos and in the 3D images a part of crinoid stem is visible, which is formed by 4 connected columns (pluricolumnal; indicated by white arrows).

In the orthophotos is noticeable a five-part radial symmetry, in particular resp. the pentagonal shape of columnals. Dimensions of the fossil: total length 2.45 mm, diameter 0.993 mm, height of one segment 0.377 mm.

P62 ?Invertebrata indet

Unidentified organic object. When viewed in orthophotos, the object has a slightly curved, cylindrical shape with a length of around 2 mm. In cross-section, it appears more circular in shape. The central part of the object is filled with a solid substance, while the surface appears more structured, with free spaces or cavities, arranged in transverse sections in a (semi)circular, arc-shaped pattern (with indications of gradual enlargement?).

The 3D photographs show that the surface of the object is more complex with many cavities (images on the right). One end of the object seems more rounded, while the other end has a slight depression (with unclear symmetry).

Px1

?Gastropoda indet

An object, which is roughly oval-shaped, has a circular outline and appears approximately spherical. This can be observed both in orthophotos and 3D images, and has a diameter of 0.684 mm. In the orthophotos, the object appears to be hollow inside (cf. red views). There are two visible holes, one located roughly in the middle with a hexagonal to circular outline, and the other one is located closer to the edge of the object with a more crescent-like shape.

Inside this second hole, there are poorly visible and indistinct internal structures resembling radial, slightly curved, thin, and parallel lamellae. The 3D images (Px1) provide almost no additional relevant information for a more precise determination of the object, except for the slight indications of an indistinct spiral structure in the image located in the centre of the upper-left corner and the image located on the bottom-left.

Px2

*unidentified organic object*

In the orthoimages, there is an elongated, almost cylindrical, roughly bilaterally symmetrical object with a length of 1.43 mm. It is open at one end and rather closed at the other one. Inside, there is a central cavity, whose diameter in the cross-section is about 1/3 of the total diameter of the element.

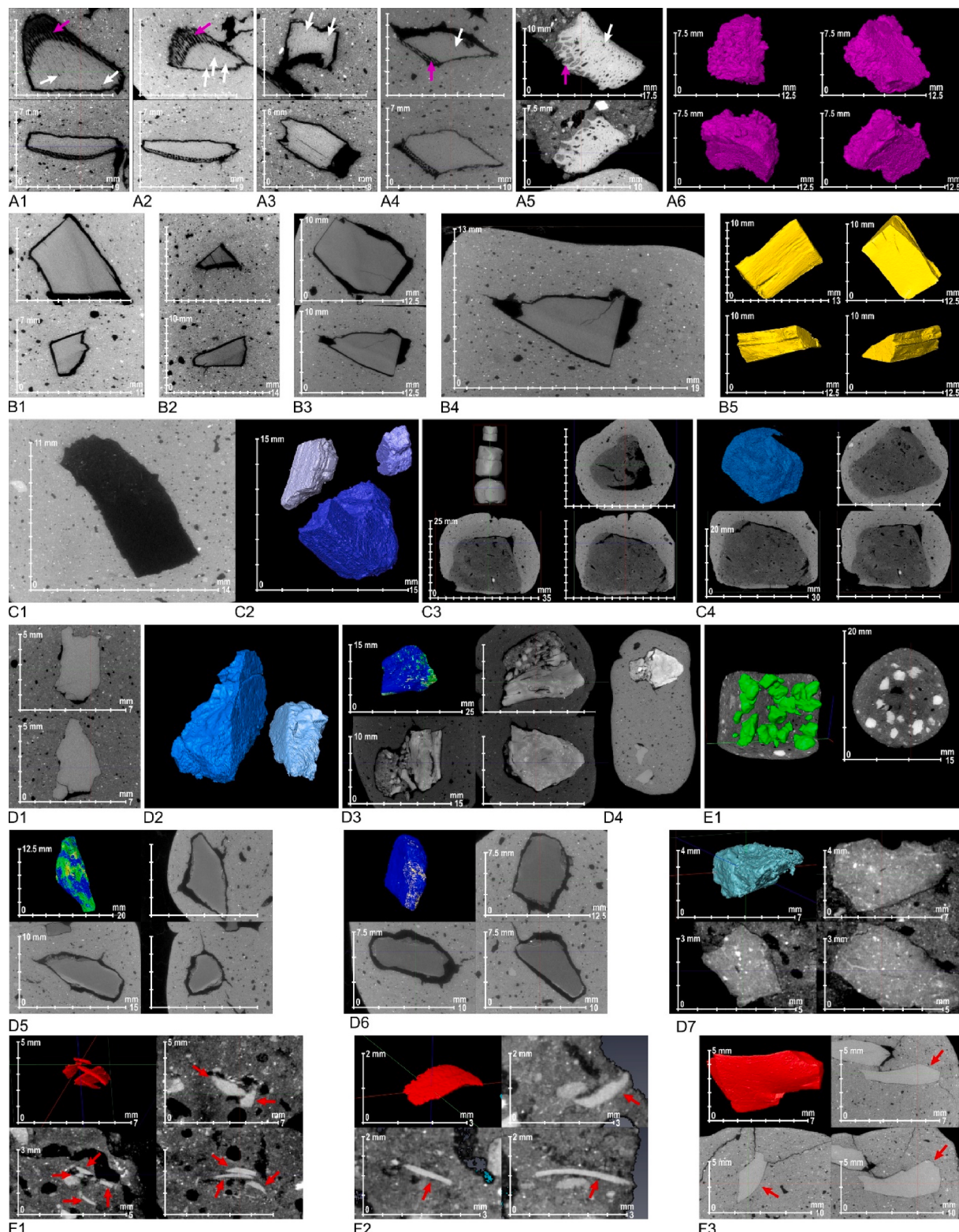
In the middle of the cavity, there is a distinct "rod-like" structure: at the open end of the object, its first roughly quarter is thickened and pointed, the second quarter is narrowed, the third quarter irregularly expands and fills almost the entire internal cavity of the object, and the last quarter is again somewhat narrowed (its diameter is roughly the same as the diameter of the tapered part). In the 3D images, a segmented structure of the inner surface of the central cavity and the tapered part of the rod-like structure are visible.

Px4

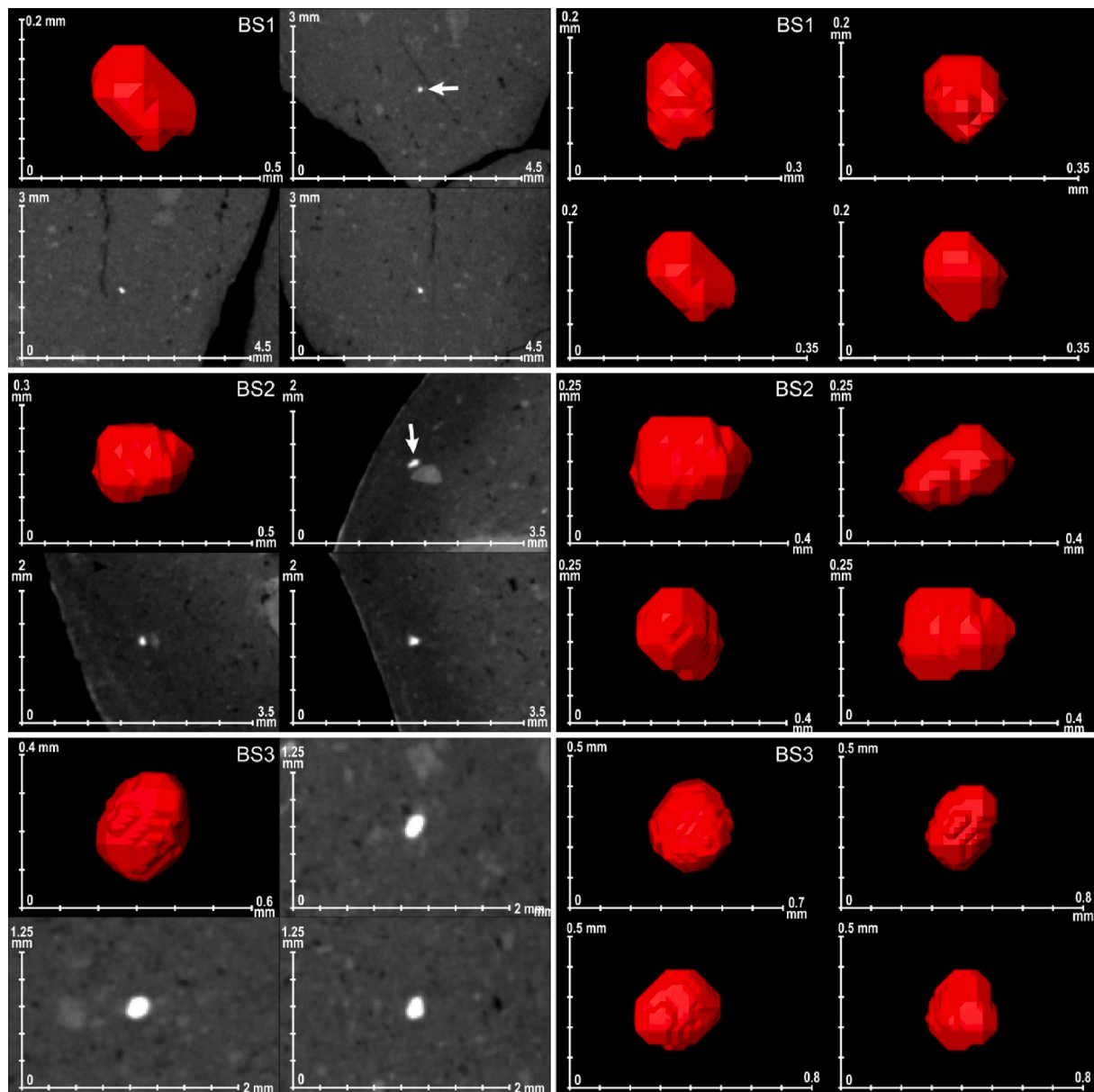
*Phylum: ?Echinodermata indet. (echinoderms)*

An object of rod-like shape, hollow inside, dimensions approximately  $1.2 \times 0.3$  mm, in the 3D image there is an indication of segmentation

(comparable to samples P29 and P39) and an inner canal.



**Appendix B Fig. 8.** Reference raw materials in phantoms. A1-A3 – orthoslices of a fresh bone (heating temperature of burning 400 °C), A4 – cf. A1 (600 °C), A5 – orthoslices of a bone from an original Gravettian layer (not burnt phantom), A6 – a segmented model of A5 (pink). White arrows indicate bone pores, pink arrows a cancellous bone. B1–B2 – orthoslices an elephant ivory (400 °C), B3–B4 – orthoslices of an ivory (600 °C), a segmented 3D model of A1; C1 – orthoslice of a mesolithic charcoal in Phantom 3 (600 °C), C2 – a segmented model of C1, C3–C4 – orthoslices and a segmented 3D model charcoal from an original gravettian layer; D1-D2 – orthoslices and segmented 3D model of quartz fragments (600 °C), D3 – a hematite from an original Gravettian layer (600 °C), D4 – the comparison of D1 (lower part) and D3 (upperpart) in Phantom 6, D5-D7 – orthoslices and segmented 3D models of rocks from an original Gravettian layer (600 °C), D7 – a porphyritic rock from an original Gravettian layer (not burnt); E1 – carbonate nodules from Dolní Věstonice site loess; F1–F3 – orthoslices and segmented models (red models and arrows) chipped chips from an original Gravettian layer (F1–F2; not burnt) and experimentally made small flake (F3; 600 °C).



**Appendix B Fig. 9.** Segmented 3D model of bright spots (small examples indicated by white arrows). It is likely that the bright spots are heavy minerals as they exhibit crystal-like shapes. Orthoviews: XY (right top), XZ (right bottom), YZ (left bottom).

### Appendix C. Supplementary data

Supplementary data to this article can be found online at <https://doi.org/10.1016/j.jas.2024.106034>.

### References

- Absolon, K., 1929. An amazing palaeolithic "pompeii" in Moravia: II. Revelations concerning the mammoth-hunters of central Europe. *The Illustrated London News* November 30, 934–938.
- Absolon, K., 1938a. Die Erforschung der diluvialen Mammutjäger-Station von Unter-Wisternitz an den Pollauer Bergen in Mähren. *Arbeitsbericht über das erste Jahr, 1924, Studien aus dem Gebiete der allgemeinen Karstforschung, der wissenschaftlichen Höhlenkunde, der Eiszeitforschung und den Nachbargebieten, Palaeoethnologische Serie 5*, Barvíč & Novotný, Brünn.
- Absolon, K., 1938b. Die Erforschung der diluvialen Mammutjäger-Station von Unter-Wisternitz an den Pollauer Bergen in Mähren. *Arbeitsbericht über das zweite Jahr 1925, Studien aus dem Gebiete der allgemeinen Karstforschung, der wissenschaftlichen Höhlenkunde, der Eiszeitforschung und den Nachbargebieten, Palaeoethnologische Serie 6 (9)*. Barvíč & Novotný, Brünn.
- Absolon, K., Zapletal, K., 1945. Výzkum diluvialní stanice lovčů mamutů v Dolních Věstonicích na Pavlovských kopcích na Moravě : pracovní zpráva za třetí rok 1926. Sdělení z paleolitického oddělení Moravského zemského muzea, Barvíč & Novotný, Brno.
- Anderson, T., Fell, C., 1995. Analysis of roman cremation vessels by computerized tomography. *J. Archaeol. Sci.* 22, 609–617. [https://doi.org/10.1016/S0305-4403\(95\)80146-4](https://doi.org/10.1016/S0305-4403(95)80146-4)
- Applbaum, N., Applbaum, Y.H., 2005. The use of medical computed tomography (CT) imaging in the study of ceramic and clay archaeological artifacts from the ancient near east. In: Uda, M., Demortier, G., Nakai, I. (Eds.), *X-Rays for Archaeology*. Springer Netherlands, Dordrecht, pp. 231–245.
- Berg, I., Ambers, J., 2016. Radiography of archaeological ceramics. In: Hunt, A. (Ed.), *The Oxford Handbook of Archaeological Ceramic Analysis*. Oxford University Press.
- Bernardini, F., Leghissa, E., Prokop, D., Velušček, A., De Min, A., Dreossi, D., Donato, S., Tuniz, C., Princivalle, F., Montagnari Kokelj, M., 2019. X-ray computed microtomography of Late Copper Age decorated bowls with cross-shaped foots from central Slovenia and the Trieste Karst (North-Eastern Italy): technology and paste

- characterisation. *Archaeological and Anthropological Sciences* 11, 4711–4728. <https://doi.org/10.1007/s12520-019-00811-w>.
- Bougard, E., 2011. Les céramiques gravettiennes de Moravie : derniers apports des recherches actuelles. *L'Anthropologie* 115, 465–504. <https://doi.org/10.1016/j.anthro.2011.05.007>.
- Braun, D.P., 1982. Radiographic analysis of temper in ceramic vessels: goals and initial methods. *J. Field Archaeol.* 9, 183–192. <https://doi.org/10.2307/529476>.
- Britannica, T.E.O.E., 2010. loess. August 13 Encyclopedia Britannica. Access date: 21.11. <https://www.britannica.com/science/loess>.
- Cărciumaru, M., Nițu, E.-C., Obadă, T., Cîrstina, O., Covalenco, S., Lupu, F.I., Leu, M., Nicolae, A., 2019. Personal ornaments in the mid upper palaeolithic east of the carpathians. PALEO - Revue d'archéologie préhistorique 30, 80–97. <https://doi.org/10.4000/paleo.4446>.
- Carr, C., 1990. Advances in ceramic radiography and analysis: applications and potentials. *J. Archaeol. Sci.* 17, 13–34. [https://doi.org/10.1016/0305-4403\(90\)90013-U](https://doi.org/10.1016/0305-4403(90)90013-U).
- Carr, C., 1993. Identifying individual vessels with X-radiography. *Am. Antiq.* 58, 96–117. <https://doi.org/10.2307/281456>.
- Carr, C., Komorowski, J.-C., 1990. Nondestructive evaluation of the mineralogy of rock temper in ceramics using X-radiography. *MRS Proceedings* 185, 435. <https://doi.org/10.1557/PROC-185-435>.
- ČÚZK, 2017. Prohlížecí služba WMS - DMR 5G (Stínovaný model reliéfu). In: Český Úřad Zeměměřický a Katastrální, 2017-05-29.
- ČÚZK, 2021. Prohlížecí služba WMS - ZABAGED®. In: Český Úřad Zeměměřický a Katastrální, 2021-12-21.
- Einwögerer, T., Simon, U., 2008. Die gravettienfundstelle krems-wachtberg. *Archäologie Österreichs* 19, 38–42.
- Farbstein, R., Davies, W., 2017. Palaeolithic ceramic technology: the artistic origins and impacts of a technological innovation. *Quat. Int.* 441, 3–11. <https://doi.org/10.1016/j.quaint.2016.11.012>.
- Farbstein, R., Radić, D., Brajković, D., Miracle, P.T., 2012. First epigravettian ceramic figurines from Europe (Vela Spila, Croatia). *PLoS One* 7, e41437. <https://doi.org/10.1371/journal.pone.0041437>.
- Farbstein, R.A., Davies, W., 2015. Rediscovering paleolithic art: overlooked ceramic figurines from the pavlovian. In: Sázelová, S., Novák, M., Mizerová, A. (Eds.), *Forgotten Times and Spaces*, Institute of Archeology of the Czech Academy of Sciences, Brno. v.v.i. and Masaryk University, Brno, pp. 328–339.
- Fiori, M.G., Nunzi, M.G., 1995. The earliest documented applications of X-rays to examination of mummified remains and archaeological materials. *J. R. Soc. Med.* 88, 67–69.
- Flügel, E., 2004. *Microfacies of Carbonate Rocks. Analysis, Interpretation and Application*. Springer Berlin, Heidelberg.
- Gait, J., Bajnok, K., Szilágyi, V., Szentí, I., Kukovecz, Á., Kis, Z., 2022. Quantitative 3D orientation analysis of particles and voids to differentiate hand-built pottery forming techniques using X-ray microtomography and neutron tomography. *Archaeological and Anthropological Sciences* 14, 223. <https://doi.org/10.1007/s12520-022-01688-y>.
- García Diez, M., 2005. Chapter IV.1. Catalogue of worked ceramic pieces. In: Svoboda, A. J. (Ed.), Pavlov I SouthEast. A Window into the Gravettian Lifestyle, the Dolní Věstonice Studies, 14, pp. 399–414. Brno.
- Gonyševová, M., 1999. Experimental reconstruction of Gravettian pottery artefacts and oven (Moravia, Czech Republic). *L'Anthropologie* 103, 519–530.
- Händel, M., Simon, U., Einwögerer, T., Neugebauer-Maresch, C., 2009. New excavations at Krems-Wachtberg – approaching a well-preserved Gravettian settlement site in the middle Danube region. *Quartar* 56, 187–196. <https://doi.org/10.7485/QU56.11>.
- Hladilová, Š., 2011. Chapter II.6. Tertiary and quaternary molluscs from Pavlov VI. In: Svoboda, A.J. (Ed.), Pavlov. Excavations 2007–2011, the Dolní Věstonice Studies, 18, pp. 54–60. Brno.
- Hložek, M., Krupa, P., Kříštek, J., 2008. Aplikace Počítacové Tomografie (CT) V Archaeologii, Antropologii a Konzervaci, Muzea, Památky, Konzervace. Technické muzeum v Brně, Brno.
- Holzknecht, M., Hamršík, B., 1988. Mikrofauna malmu ve vrtu Nové Mlýny – 3 (jižní Morava, ČSSR). *Miscellanea micropaleontologica* 16, 21–59.
- Houša, V., Scheibner, E., Stráník, Z., 1963. Tithonian stratigraphy of west carpathians. *Geol. Sb.* 14, 3–17.
- Hughes, S., 2011. CT scanning in archaeology. In: Luca, S. (Ed.), *Computed Tomography*. IntechOpen, Rijeka, pp. 57–70.
- Hunter, A.W., Underwood, C.J., 2009. Palaeoenvironmental control on distribution of crinoids in the bathonian (middle jurassic) of england and France. *Acta Palaeontol. Pol.* 54, 77–98.
- Insoll, T., Kankpeyeng, B., Fraser, S., 2016. Internal meanings: computed tomography scanning of koma figurines from Ghana. *Afr. Arts* 49, 24–33. [https://doi.org/10.1162/AFAR\\_a\\_00264](https://doi.org/10.1162/AFAR_a_00264).
- Jarvis, A., Reuter, H.I., Nelson, A., Guevara, E., 2008. Hole-filled seamless SRTM data V4. International Centre for Tropical Agriculture (CIAT).
- Jüttner, K., 1922. Entstehung und Bau der Pollauer Berge, A. Bartosch, Nikolsburg.
- Kahl, W.-A., Ramminger, B., 2012. Non-destructive fabric analysis of prehistoric pottery using high-resolution X-ray microtomography: a pilot study on the late Mesolithic to Neolithic site Hamburg-Boberg. *J. Archaeol. Sci.* 39, 2206–2219. <https://doi.org/10.1016/j.jas.2012.02.029>.
- Kalender, W.A., 2011. *Computed Tomography: Fundamentals, System Technology, Image Quality, Applications*, third ed. John Wiley & Sons.
- Kingston, A.M., Myers, G.R., Latham, S.J., Recur, B., Li, H., Sheppard, A.P., 2018. Space-filling X-ray source trajectories for efficient scanning in large-angle cone-beam computed tomography. *IEEE Transactions on Computational Imaging* 4, 447–458. <https://doi.org/10.1109/TCI.2018.2841202>.
- Klíma, B., 1963. Dolní Věstonice. Výzkum Táboriště Lovců Mamutů V Letech 1947–1952, Monumenta Archaeologica 11. Nakladatelství Československé akademie věd, Praha.
- Klíma, B., 1981. Střední část paleolitické stanice u Dolních Věstonic. Památky archeologické 72, 5–92.
- Klíma, B., 1983. Dolní Věstonice, táboriště lovčů mamutů, 1. vyd. In: Památníky Naší Minulosti, 12. Academia, Praha.
- Knor, A., Ložek, V., Pelšek, J., Žebera, K., 1953. Dolní Věstonice. Výzkum Táboriště Lovců Mamutů V Letech 1945–1947, Monumenta Archeologica 2. Nakladatelství Československé akademie věd, Praha.
- Kozatsas, J., Kotsakis, K., Sagris, D., David, K., 2018. Inside out: assessing pottery forming techniques with micro-CT scanning. An example from Middle Neolithic Thessaly. *J. Archaeol. Sci.* 100, 102–119. <https://doi.org/10.1016/j.jas.2018.10.007>.
- Krajewski, M., Ferré, B., Salamon, M.A., 2020. Cyrtocrinids (cyrtocrinida, Crinoidea) and other associated crinoids from the jurassic (Kimmeridgian–Tithonian)–Cretaceous (Berriasian–Barremian) of the carpathian foredeep basement (western Ukraine). *Geobios* 60, 61–77.
- Králik, M., Svoboda, J., Škrda, P., Nývltová Fišáková, M., 2008. Nové nálezy keramických fragmentů a otisků v gravettienu jižní moravy. New finds of ceramic fragment and imprints in the South moravian gravettian. *Přehled výzkumu* 49, 3–22.
- Kreiter, A., 2008. A Celtic pottery kiln and ceramic technological study from Zalakomár-Alsó Csálf (S-W Hungary). *Zalai Múzeum* 17, 131–148.
- Kreiter, A., Riebe, D.J., Parkinson, W.A., Pető, Á., Tóth, M., Pánczél, P., Bánffy, E., 2014. Unique in its chaîne opératoire, unique in its symbolism: undressing a figurine from the 6th Millennium BC Körös culture, Hungary. *J. Archaeol. Sci.* 44, 136–147. <https://doi.org/10.1016/j.jas.2014.01.027>.
- Kroh, A., Lukeneder, A., 2009. Crinoids from the late jurassic of the nutzhof section (lower Austria, gresten klippenbelt. *Ann. Naturhist. Mus. Wien* 110 A, 383–399.
- Landis, E.N., Keane, D.T., 2010. X-ray microtomography. *Mater. Char.* 61, 1305–1316. <https://doi.org/10.1016/j.matchar.2010.09.012>.
- Lázníčková-Galetová, M., 2021. Gravettian ivory ornaments in central Europe, Moravia (Czech republic). *L'Anthropologie* 125, 102870. <https://doi.org/10.1016/j.anthro.2021.102870>.
- Lázníčková-Galetová, M., 2022. Nejstarší šperky a ozdoby těla. Moravské zemské muzeum, Brno.
- MAMBA, 2024. Exploring Mammoth Bone Accumulations in Central Europe. European Research Counsil. Access date: 3. 6. 2024. <https://cordis.europa.eu/project/id/101045245>.
- McGarry, C.K., Grattan, L.J., Ivory, A.M., Leek, F., Liney, G.P., Liu, Y., Miloro, P., Rai, R., Robinson, A.P., Shih, A.J., Zeqiri, B., Clark, C.H., 2020. Tissue mimicking materials for imaging and therapy phantoms: a review. *Phys. Med. Biol.* 65, 23TR01 <https://doi.org/10.1088/1361-6560/abbd17>.
- Middleton, A., 2005. Ceramics. In: Lang, J., Middleton, A. (Eds.), *Radiography of Cultural Material*. Elsevier, Amsterdam, pp. 76–95.
- Moore, R.C., 1966. Treatise on Invertebrate Paleontology, Part U – Echinodermata 3, Volume 1. The Geological Society of America, Inc. and The University of Kansas Press.
- Moore, R.C., Jeffords, R.M., 1968. Classification and Nomenclature of Fossil Crinoids Based on Studies of Dissociated Parts of Their Columns., the University of Kansas Paleontological Contributions, Serial Number 46, Echinodermata, Article 9. The University of Kansas Publications.
- Müller, A.H., 1963. II. Unterstamm Eleutherozoa Bell, 1891, Lehrbuch der Paläozoologie. Band II, Invertebraten, Teil 3 Arthropoda 2 - Stomochorda. VEB Gustav Fischer Verlag, Jena, pp. 398–547.
- Müller, A.H., 1980. Lehrbuch der Paläozoologie. Band II, Invertebraten, Teil 1 Protozoa – Mollusca 1. VEB Gustav Fischer Verlag, Jena.
- Murray, J.W., 1990. *Worbellose Makrofossilien. Ein Bestimmungsatlas*. Ferdinand Enke Verlag, Stuttgart.
- Nerudová, Z., Vaníčková, E., Tvrď, Z., Ramba, J., Bílek, O., Kostrhun, P., 2019. The woman from the Dolní Věstonice 3 burial: a new view of the face using modern technologies. *Archaeological and Anthropological Sciences* 11, 2527–2538. <https://doi.org/10.1007/s12520-018-0698-3>.
- Novák, M., Boriová, S., Herčík, O., Chláchula, D., 2022. Dolní Věstonice (okr. Břeclav). *Přehled výzkumu* 64, 147–148.
- Novák, M., Wilczyński, J., Händl, M., Boriová, S., Herčík, O., Chláchula, D., 2023. On the periphery of a mammoth "kjøkkenmödding". The new excavation of the extensive bone deposit at Dolní Věstonice I. In: 29th EAA Annual Meeting (Belfast, Northern Ireland 2023) - Abstract Book, European Association of Archaeologists, Belfast, pp. 1013–1014.
- Oliva, M., 2014. Dolní Věstonice I (1922–1942). Hans Freising - Karel Aboslon - Assien Bohmers, *Anthropos* 37 (N.S. 29). Moravské zemské muzeum, Brno.
- Oliva, M., 2015. Umění moravského paleolitu. *Atlas sbírky Ústavu Anthropos Moravského zemského muzea*, *Anthropos* 38/N.S. 30.
- Oliva, M., 2021. Mammoth remains, burials, and art (30–15 KY AGO): anthropological perspective. *Anthropologie* 59, 225–249.
- Pavel, C., Suciu, C., Constantin, F., Bugoi, R., 2013. X-ray computed tomography investigations of Cucuteni ceramic statuettes. *Documenta Prachistorica* 40, 323–332. <https://doi.org/10.4312/dp.40.26>.
- Pfeifer, S.J., Hartramph, W.L., Kahlke, R.-D., Müller, F.A., 2019. Mammoth ivory was the most suitable osseous raw material for the production of Late Pleistocene big game projectile points. *Sci. Rep.* 9, 2303. <https://doi.org/10.1038/s41598-019-38779-1>.
- Pizzeghello, A., Vidale, M., Salemi, G., Tinè, V., Di Pilato, S., 2015. De-construcing terracotta female figurines: a chalcolithic case-study. *Interdisciplinaria Archeol. Nat. Sci. Archaeol.* 6, 7–17.

- Reedy, C.L., Reedy, C.L., 2022a. High-resolution micro-CT with 3D image analysis for porosity characterization of historic bricks. *Heritage Science* 10, 83. <https://doi.org/10.1186/s40494-022-00723-4>.
- Reedy, C.L., Reedy, C.L., 2022b. Micro-computed tomography with 3D image analysis to reveal firing temperature effects on pore systems in archaeological and ethnographic ceramics. *Appl. Sci.* 12, 11448.
- Rich, S.A., 2008. Midwifery and neolithic Malta: interpreting and Contextualizing two terracotta figurines, OMERTAA. *Journal of Applied Anthropology* 2008, 260–268.
- Rye, O.S., 1977. Pottery manufacturing techniques: X-ray studies. *Archaeometry* 19, 205–211. <https://doi.org/10.1111/j.1475-4754.1977.tb00200.x>.
- Řehánek, J., 1987. Biostratigrafia a faciální vývoj karbonátového malmu jv. svahů Českého masívu. *Miscellanea micropaleontologica* 2, 251–282.
- Řehor, F., Řehorová, M., Vašíček, Z., 1978. Za zkamenělinami severní Moravy, Ostravské muzeum. Ostrava.
- Salamon, M.A., Bubík, M., Ferré, B., Duda, P., Plachno, B.J., 2021. Hrabalicrinus zitti gen. et sp. nov., and other Upper Jurassic crinoids (Echinodermata, Crinoidea) from the Brno area (Czech Republic). *Ann. Paleontol.* 107, 102482. <https://doi.org/10.1016/j.anpal.2021.102482>.
- Shepard, A.O., 1956. Ceramics for the Archaeologist. Carnegie Institution of Washington, Washington, D.C.
- Shikhaliev, P.M., 2012. Dedicated phantom materials for spectral radiography and CT. *Phys. Med. Biol.* 57, 1575–1593. <https://doi.org/10.1088/0031-9155/57/6/1575>.
- Schneider, S., Harzhauser, M., Kroh, A., Lukeneder, A., Zuschin, M., 2013. Limestone and klenitne beds (kimmeridgian – berriasian; waschberg-ždánice unit; NE Austria and SE Czech republic): state of the art and bibliography. *Bull. Geosci.* 88, 105–130.
- Soffer, O., Vandiver, P., 1994. The ceramics. In: Svoboda, J. (Ed.), *Pavlov I – Excavations 1952–53, Études et Recherches Archéologiques de l’Université de Liège* 66. Université de Liège, Liège, pp. 163–173.
- Soffer, O., Vandiver, P., 1997. The ceramics from Pavlov I-1957 excavation. In: Svoboda, J. (Ed.), *Pavlov I – Northwest. The Upper Paleolithic Burial and its Settlement Context, the Dolní Věstonice Studies 4*, Institute of Archaeology AS CR Brno, Brno, pp. 383–401.
- Soffer, O., Vandiver, P., 2005. Chapter IV.2. Ceramic fragments. In: Svoboda, A.J. (Ed.), *Pavlov I SouthEast. A Window into the Gravettian Lifestyle, the Dolní Věstonice Studies*, 14, pp. 415–431. Brno.
- Svoboda, J., Králík, M., Culíková, V., Hladilová, S., Novák, M., Fisáková, M., Nývlt, D., Zelinková, M., 2009. Pavlov VI: an upper palaeolithic living unit. *Antiquity* 83, 282–295.
- Svoboda, J., Novák, M., Sázelová, S., Hladilová, Š., Škrda, P., 2018. *Dolní Věstonice I. Excavations 1990–1993. Přehled výzkumu* 59, 35–67.
- Svoboda, J.A., 2020. *Dolní Věstonice – Pavlov. Explaining Paleolithic Settlements in Central Europe*. Texas A&M University Press, College Station.
- Titterington, P.F., 1935. Certain bluff mounds of western Jersey county, Illinois. *Am. Antq.* 1, 6–46. <https://doi.org/10.2307/275856>.
- Van Beek, G., 1969. *Hajar Bin Humeid. Investigations at a Pre-islamic Site in South Arabia*. John Hopkins Press, Baltimore.
- Vandiver, P.B., Soffer, O., Klima, B., Svoboda, J., 1989. The origins of ceramic technology at dolni-vestonice, czechoslovakia. *Science* 246, 1002–1008.
- Varslot, T., Kingston, A., Myers, G., Sheppard, A., 2011. High-resolution helical cone-beam micro-CT with theoretically-exact reconstruction from experimental data. *Med. Phys.* 38, 5459–5476. <https://doi.org/10.1118/1.3633900>.
- Vigorelli, L., Re, A., Buscaglia, P., Manfreda, N., Nervo, M., Cavalieri, T., Del Vesco, P., Borla, M., Grassini, S., Guidorzi, L., Lo Giudice, A., 2022. Comparison of two ancient Egyptian Middle Kingdom statuettes from the Museo Egizio of Torino through computed tomographic measurements. *J. Archaeol. Sci.: Report* 44, 103518. <https://doi.org/10.1016/j.jasrep.2022.103518>.
- Weber, G.W., Lukeneder, A., Harzhauser, M., Mitteroecker, P., Wurm, L., Hollaus, L.-M., Kainz, S., Haack, F., Antl-Weiser, W., Kern, A., 2022. The microstructure and the origin of the Venus from Willendorf. *Sci. Rep.* 12, 2926. <https://doi.org/10.1038/s41598-022-06799-z>.
- Wolf, S., Vercoutère, C., 2018. L’exploitation de l’ivoire de Mammouth au Paléolithique. *L’Anthropologie* 122, 579–587. <https://doi.org/10.1016/j.anthro.2017.09.001>.
- Zhel'tova, M., Yanshina, O., 2015. "Ceramics" and pigments from kostienki-1 site: research and perspectives. In: Sázelová, S., Novák, M., Mizerová, A. (Eds.), *Forgotten Times and Spaces: New Perspectives in Paleoanthropological, Paleoethnological and Archeological Studies*. Institute of Archeology of the Czech Academy of Sciences & Masaryk University, Brno, Brno, pp. 340–346.
- Žitt, J., Michalík, J., 1984. Upper jurassic crinoids in the west carpathian klippen belt. *Geol. Carpathica* 35, 601–629.